Chapter 5: Deformation Behavior and Tribo-Mechanical Properties of the Complex Hypoeutectic Al-7.4Si-2.5Cu-0.6Fe alloy during Forging

5.1 Introduction

In view of the earlier discussion in previous chapters it is evident that the microstructural features of the Al-Si alloy changes by varying the amount Si wt.%, and consequently the bulk processing of the Al-Si alloy becomes difficult due to the presence of Si in the Al matrix. The hypereutectic Al-Si alloy comprises of primary and eutectic Si grains whereas hypoeutectic composition contains needle and plate-shaped eutectic Si particles. Such Si particles produce surface cracks in the products during bulk processing. In the present study, the amount (wt.%) of Si is reduced from 11 to 7.4 wt.% in the Al-Si alloy (Al-7.4Si-2.5Cu-0.6Fe) and the deformation behavior was analyzed during bulk processing. The alloy forged through open die set, impression die set and converging die under different processing conditions of aspect/reduction ratios, working temperatures, and interfacial frictional conditions. Thus, it is expected that the present work shall provide valuable insight into understanding the deformation behavior and tribo-mechanical characteristics of the Al-7.4Si-2.5Cu-0.6Fe (wt.%) alloy under different processing conditions.

5.2 Results and Discussion

5.2.1 Microstructural features of the as-cast alloy

Figure 5.1 shows the X-ray diffraction patterns of as-cast Al-7.4Si-2.5Cu-0.6Fe alloy. The diffraction pattern mainly comprises high intensity peaks of Al and Si phases. However, formation of intermetallic compounds (Al_2Cu and β-$Al_{4.5}FeSi$) were also confirmed from the

XRD patterns, and their peaks were very low. The formation of intermetallic phases may be attributed to high temperature during process run over and higher exposure stimulates interfacial reactions between Al and alloying elements Si, and Cu.

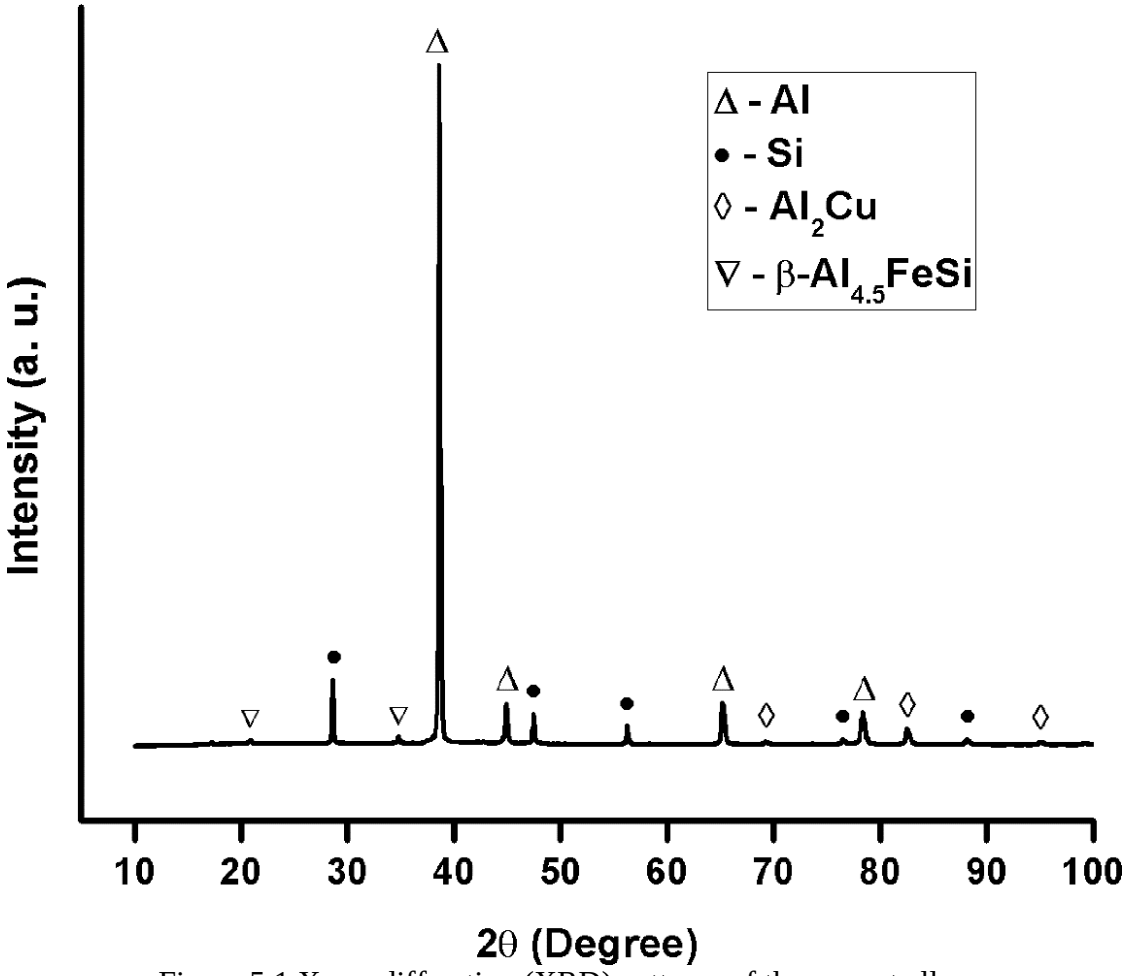

Figure 5.1 X-ray diffraction (XRD) patterns of the as-cast alloy

The energy dispersive x-ray (EDS) spectrum of the as-cast alloy was taken from area observed in the SEM images as shown in Figure 5.2. The EDS analysis indicates the presence of the Al, Si, Cu, Fe, Mg and Zn elements (Figure 5.2(a)) in the alloy. EDS spectrum further confirmed the formation of intermetallic compounds β-$Al_{4.5}FeSi$ and Al_2Cu (Figures 5.2(b), and 5.2(d)) during solidification. These compounds were present in the matrix in plate type and coarse needle-shaped morphology. Figure 5.2(c), shows the EDS spectrum of Si crystal.

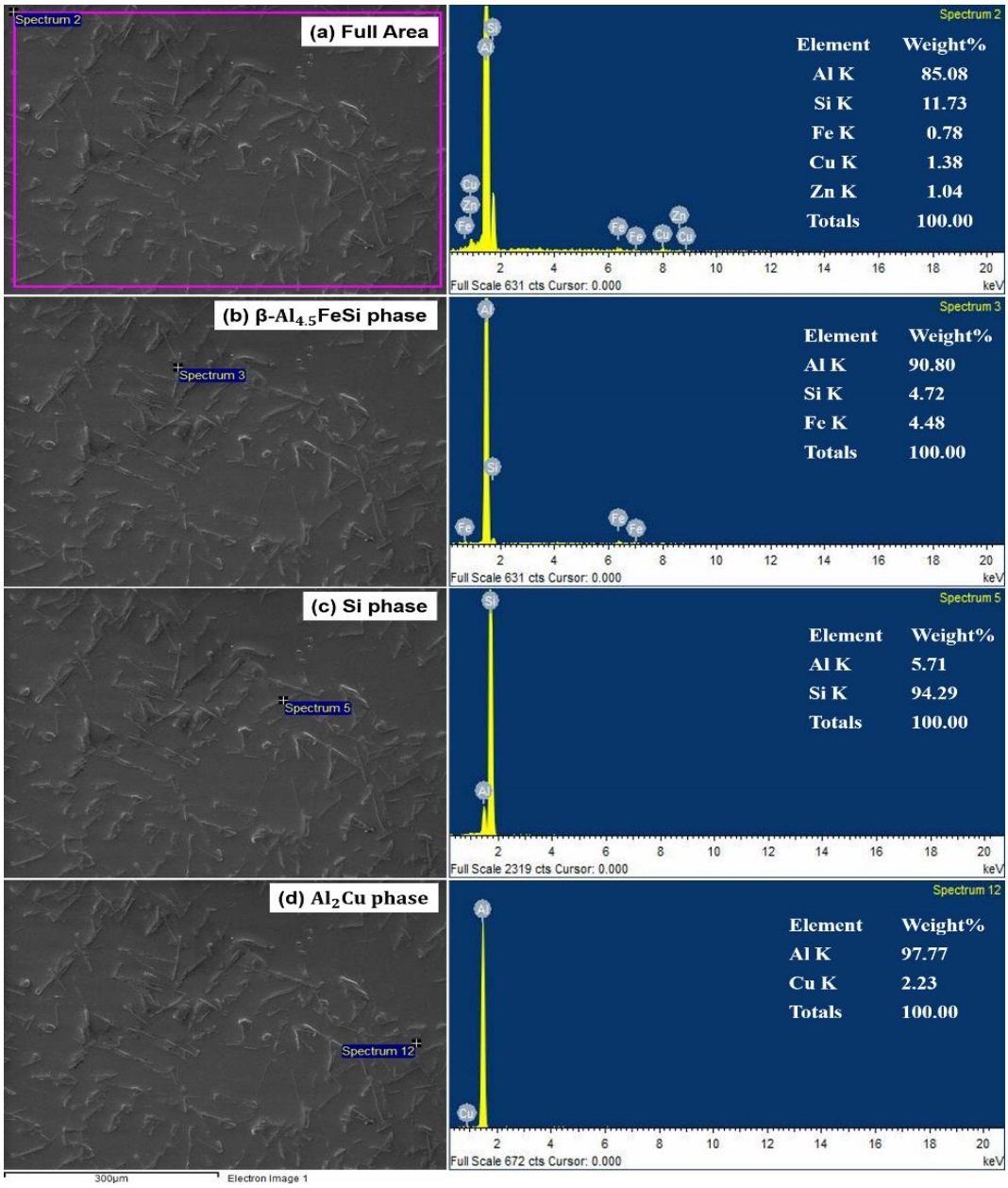

Figure 5.2 EDS analysis of the as-cast alloy

Figures 5.3(a) and 5.3(b) show the optical and SEM micrographs of as-cast Al-7.4Si-2.5Cu-0.6Fe alloy. The optical microstructure Figure 5.3(a) shows irregular and coarse needle shaped eutectic silicon phases were randomly oriented and non-uniformly distributed in the α-Al matrix. Along these phases few plate and needle shaped intermetallic compounds were also present in the matrix as depicted in the SEM micrograph, Figure 5.3(b). The formation

and distribution of such microstructural features occurred in the cast alloy due to non-uniformity in cooling rate during solidification process. The mean diameter and standard deviation of the eutectic silicon particles were measured as 25.33 µm and 15.02 µm respectively. The presence of coarse needle-shaped eutectic silicon particles and intermetallic phases is the major drawback of the cast alloy. The alloy having such microstructural features deteriorate mechanical properties and tribological characteristics of the alloy. These second phase particles act as the primary nucleating sites for cracks during straining, and thus the material fails before reaching the intrinsic strength under severe working conditions. Therefore, the material with desired mechanical and metallurgical properties can be achieved by modifying such deleterious microstructural features of the as-cast alloy. In earlier, various authors have reported similar trends in Al-Si alloy with different composition (Zhu et al., 2012; and Samuel et al., 2015).

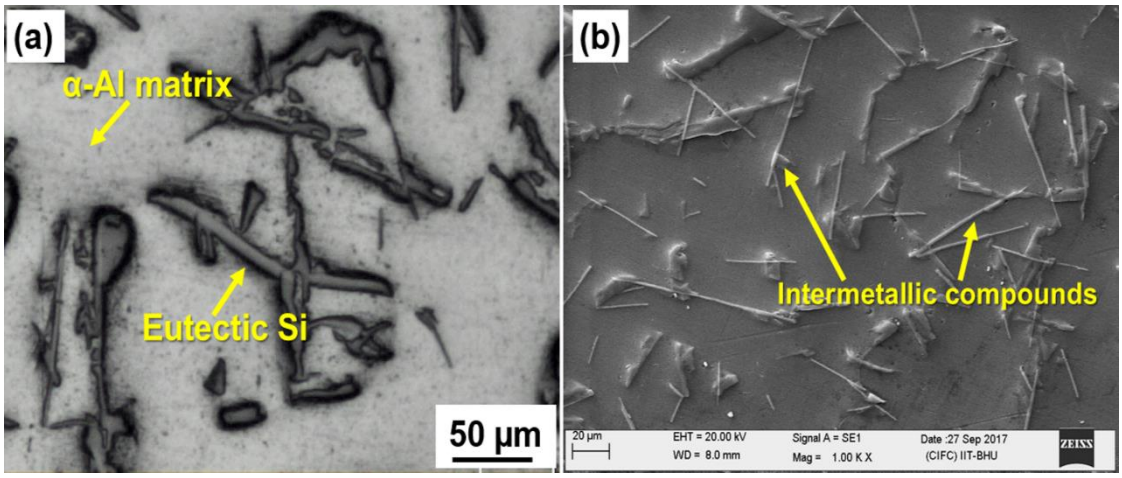

Figure 5.3 Micrograph of the cast A356 aluminum alloy (a) optical, and (b) SEM

5.2.2 Deformation behavior of the complex hypoeutectic Al-7.4Si-2.5Cu-0.6Fe alloy forged under different die sets

The deformation behavior of the complex hypoeutectic Al-7.4Si-2.5Cu-0.6Fe alloy has been investigated during forging under various processing conditions. The different dies such as

open die, impression die, and converging die sets have been used for the bulk processing of the alloy under various processing temperatures.

5.2.2.1 Deformation behavior of the complex hypoeutectic Al-Si alloy during open die forging

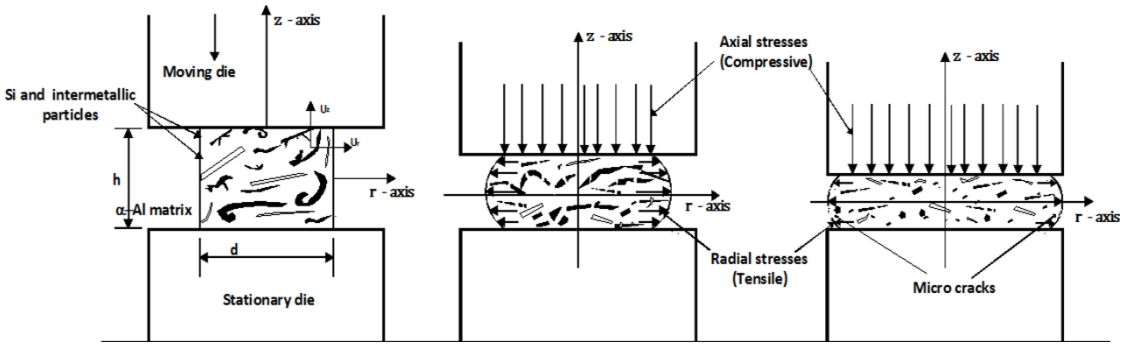

Figure 5.4 Three regimes of silicon-intermetallic particles distribution with aluminum matrix during open die forging of the complex Al-Si alloy

The open die forging of the test samples (h/d=1) were performed under similar processing conditions as used in previous section 3.2.2.1. Figure 5.4 shows the three regimes of silicon-intermetallic particles distribution in the aluminum matrix during open die forging of Al-Si alloy. The results reveal that minute micro surface cracks were developed on the outer periphery of the test samples during open die forging of the alloy in both room and elevated working temperatures (300°C) as shown in Figures 5.5(a-b). It may be due to the presence of hard eutectic Si and intermetallic phases act as the primary nucleating sites for micro cracks during straining. At room temperature the insufficient recovery of the material and greater deformation load initiates micro cracks, whereas incomplete recovery of the material at 300°C initiates very minute micro cracks between second phase particles and α-Al matrix. Due to no restriction of the outward metal flow in open die condition promotes further propagation of these micro cracks on the outer periphery of the test samples. Therefore, as the deformation proceeds several fine micro cracks were formed on the outer periphery

surface of the test samples. Although the open die forging of the above alloy produces very minute cracks on the forged products, and this can be easily removed by machining of the outer surfaces. Therefore, secondary process (machining) required to obtain forged products without surface defects. This increases the cost of the products as well as production time to get a desired products.

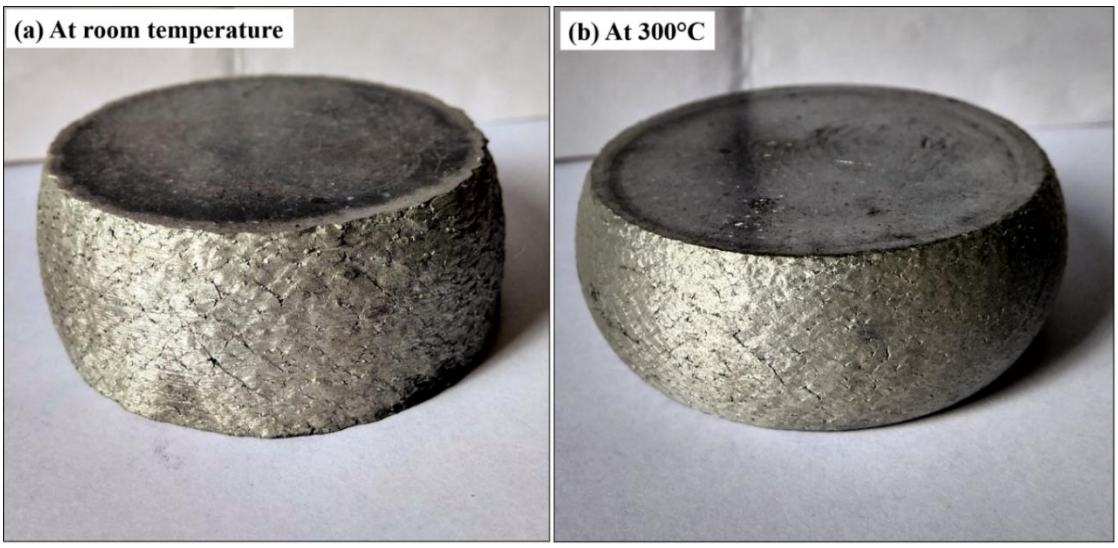

Figure 5.5 Open die forged products under different working condition (a) room temperature, (b) 300°C

5.2.2.2 Deformation behavior of the complex hypoeutectic Al-Si alloy during impression die forging at room temperature

Impression die forging of the test samples with different aspect ratios performed under similar processing conditions as used in section 3.2.2.2. Figures 5.6(a-b) and 5.7 show the photograph of cold forged products and their corresponding forging load under lubricated and unlubricated interfacial frictional conditions at 0.80, 1.00 and 1.20 aspect ratios. The results reveal that crack free product obtained through impression die forging of the alloy at cold condition. As discussed in previous section that micro cracks were formed on the surface of the forged products in open die condition due to no restriction of the outward metal flow. However, in impression die forging the outward metal flow gets restricted through die wall

which in turn control the propagation of the micro cracks. In between back stresses produced through die wall during forging are quite sufficient to suppress the above micro cracks and protect against any surface defect. Therefore, defect free products were obtained through forging of the alloy in impression die at room temperature in both lubricated conditions as shown in Figure 5.6. The results show that test sample forged at lubricated condition show better surface finish as compared to unlubricated condition. It may be due to the fact that lubrication reduced the friction between contacting die wall and test samples and allow the deformation to proceed. It also reduced the deformation load in lubricated condition, while considerably greater load was required to deform the material against friction as shown in Figure 5.7.

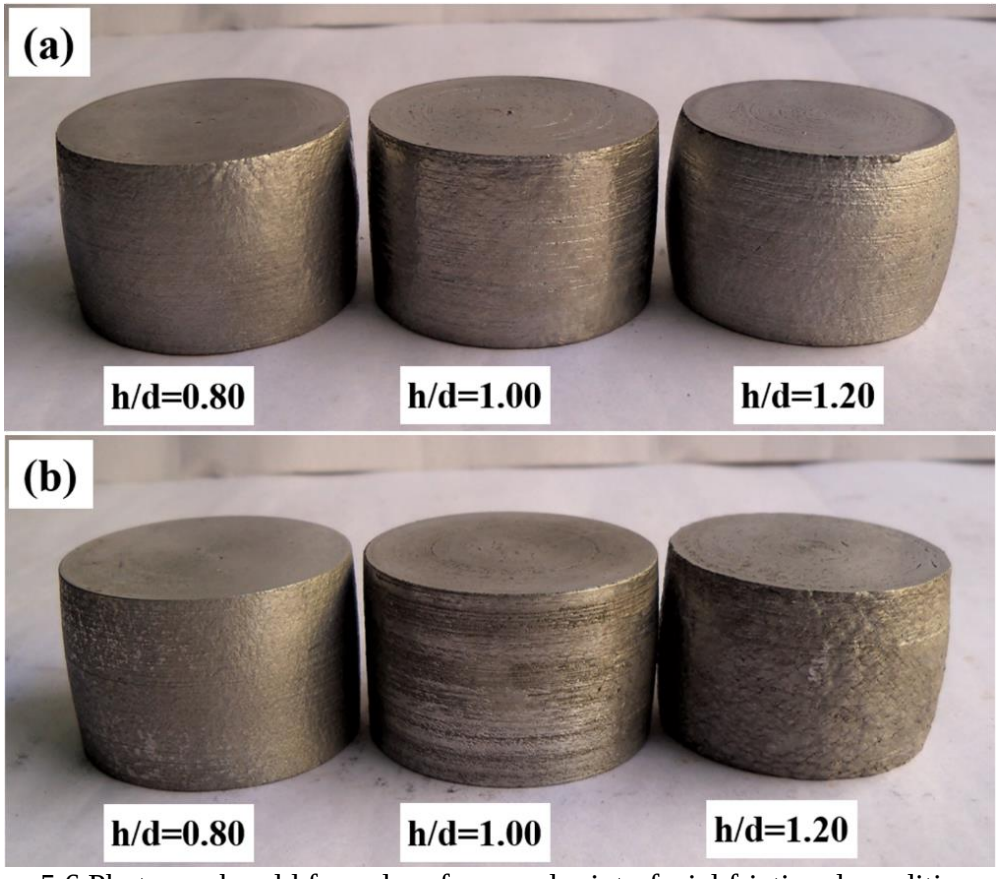

Figure 5.6 Photograph cold forged preform under interfacial frictional conditions with different aspect ratios (a) lubricated, and (b) unlubricated

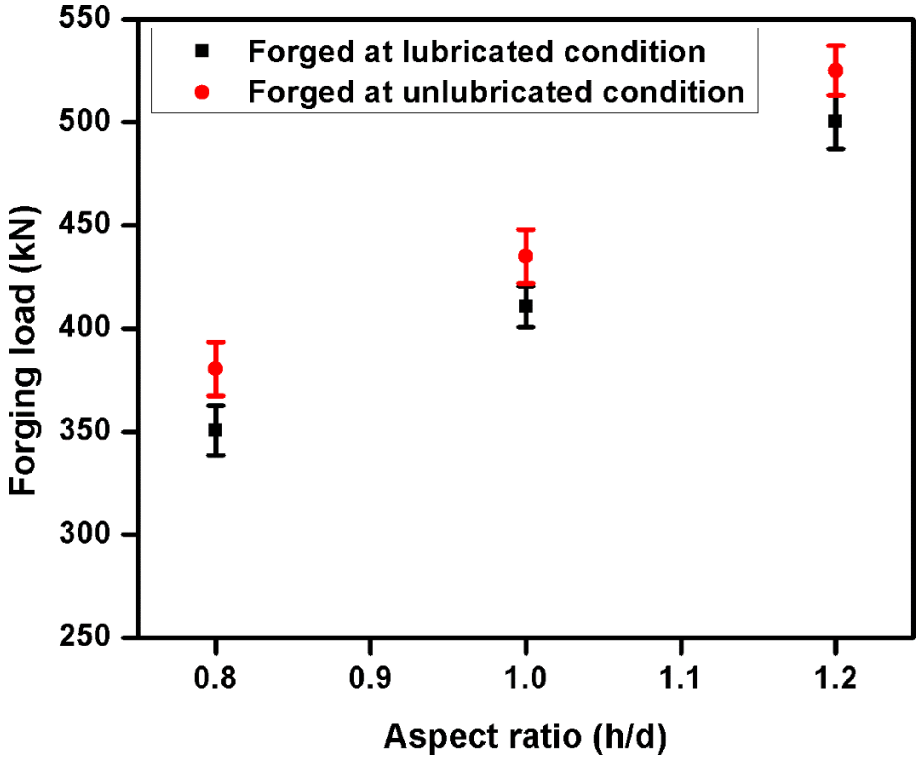

Figure 5.7 Variation of forging load with aspect ratio (h/d) at lubricated and lubricated conditions

In view of the above discussion, it is established that the impression die forging of the complex Al-7.4Si-2.5Cu-0.6Fe alloy at room temperature and defect free products can obtained through bulk processing.

5.2.2.3 Deformation behavior of the complex hypoeutectic Al-Si alloy during impression die forging at elevated working temperatures

The impression die forging of the test samples were performed through power hammer at elevated temperatures 300, 400, and 500°C under lubricated and unlubricated interfacial frictional conditions. Similar results were obtained during bulk processing of the alloy through impression die at elevated temperatures as reported in the previous section 3.2.2.4 and 4.2.2.4. The results reveal that the defect free forged products were found during forging of the alloy at elevated temperature in both lubricated and unlubricated interfacial friction conditions, as shown in Figures 5.8 and 5.9. Due to less friction between contacting surfaces

the test samples forged at lubricated conditions show better surfaces finish as compared with unlubricated ones. The friction force between contacting surfaces reflect the greater deformation load during forging of the alloy at unlubricated conditions as shown in Figures 5.10 and 5.11.

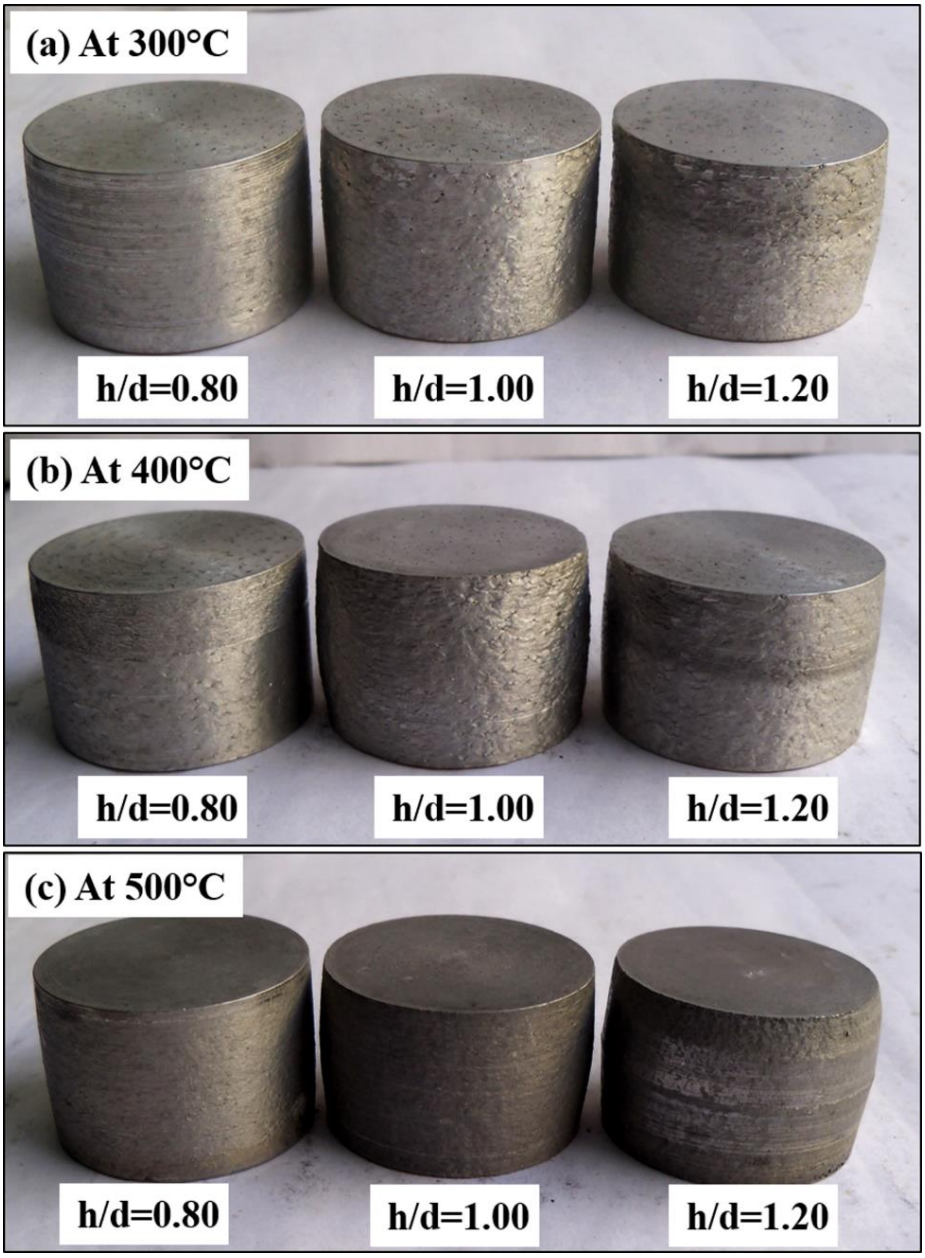

Figure 5.8 Photograph of impression die forged products under lubricated condition at elevated processing temperature (a) 400°C, (b) 400°C, and (c) 500°C

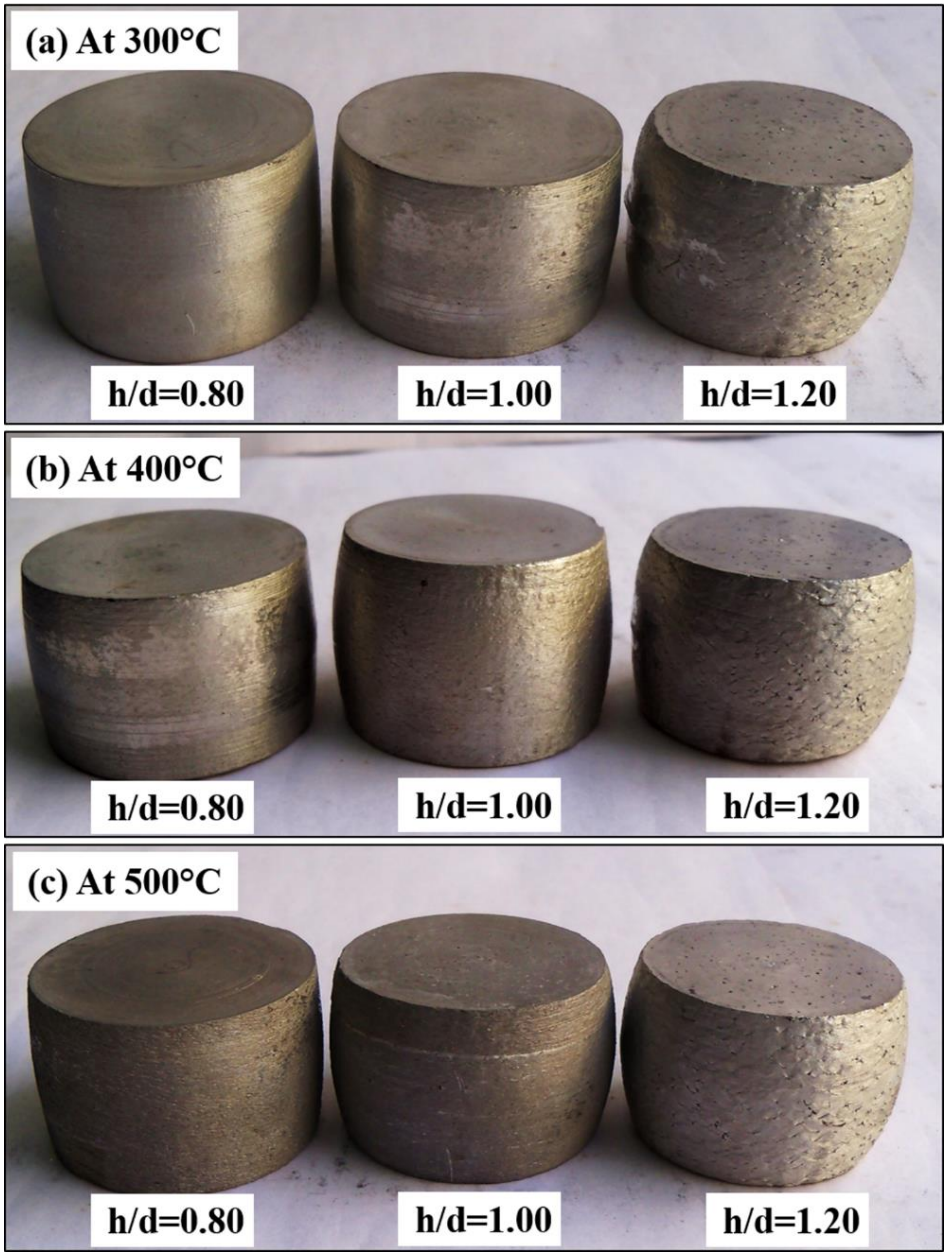

Figure 5.9 Photograph of impression die forged products under unlubricated condition at elevated processing temperature (a) 400°C, (b) 400°C, and (c) 500°C

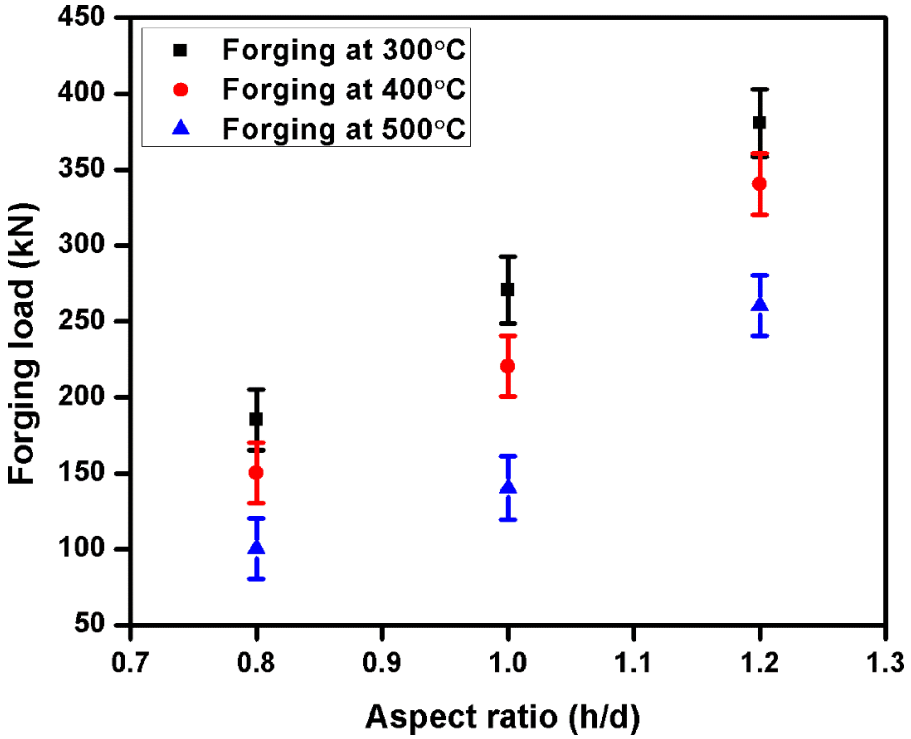

Figure 5.10 Variation of forging load with aspect ratio (h/d) at different working temperatures under lubricated condition

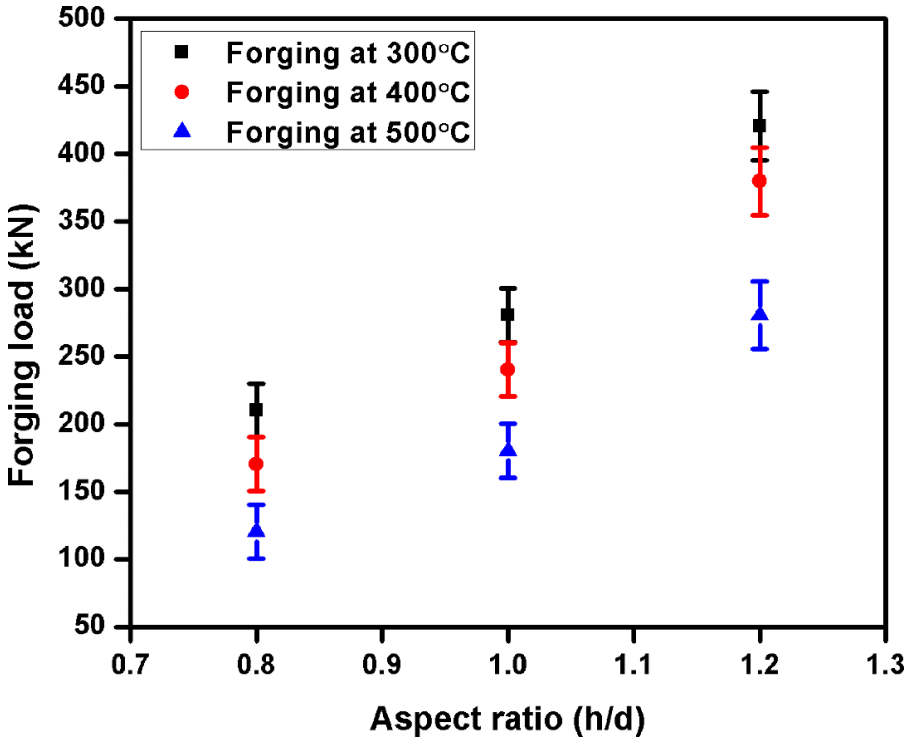

Figure 5.11 Variation of forging load with aspect ratio (h/d) at different working temperatures under unlubricated condition

The above results reveal that bulk processing of the complex Al-7.4Si-2.5Cu-0.6Fe alloy through impression die forging was feasible and defect free forged products can be produced.

5.2.2.4 Deformation behavior of the complex hypoeutectic Al-Si alloy during converging die forging

Converging die forging of the complex hypoeutectic Al-7.4Si-2.5Cu-0.6Fe was done using two different reduction ratios of 1.5 and 2.0 at 300, 400, and 500°C elevated temperatures under lubricated condition.

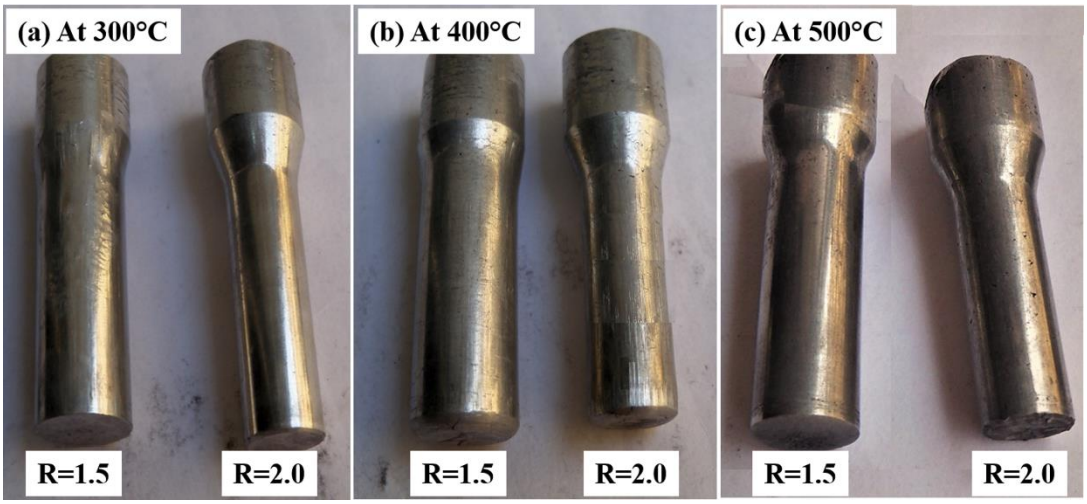

Figure 5.12 Photographs of forged products at various elevated working temperatures (a) 300°C, (b) 400°C, and (c) 500°C

The photograph of forged products and corresponding forging load under various processing conditions are shown in Figures 5.12(a-c) and 5.13, respectively. The results of converging die forging shows similar trends as discussed in section 4.2.2.4. Here also the billets forged at low working temperatures and reduction ratio (1.5) show better surface finish as compared with other processing conditions as shown in Figure 5.12. Also, the billets forged at low working temperatures and higher reduction ratio demand high forging load during bulk processing as shown in Figure 5.13. Due to severe deformation of the alloy during converging die forging, the coarse hard second phase particles got fragmented, and uniformly

dispersed in the α-Al matrix. Therefore, fine second phase particles reoriented in the matrix and formed strong structure during converging die processing, which consequently enhances the mechanical and wear performance of the alloy.

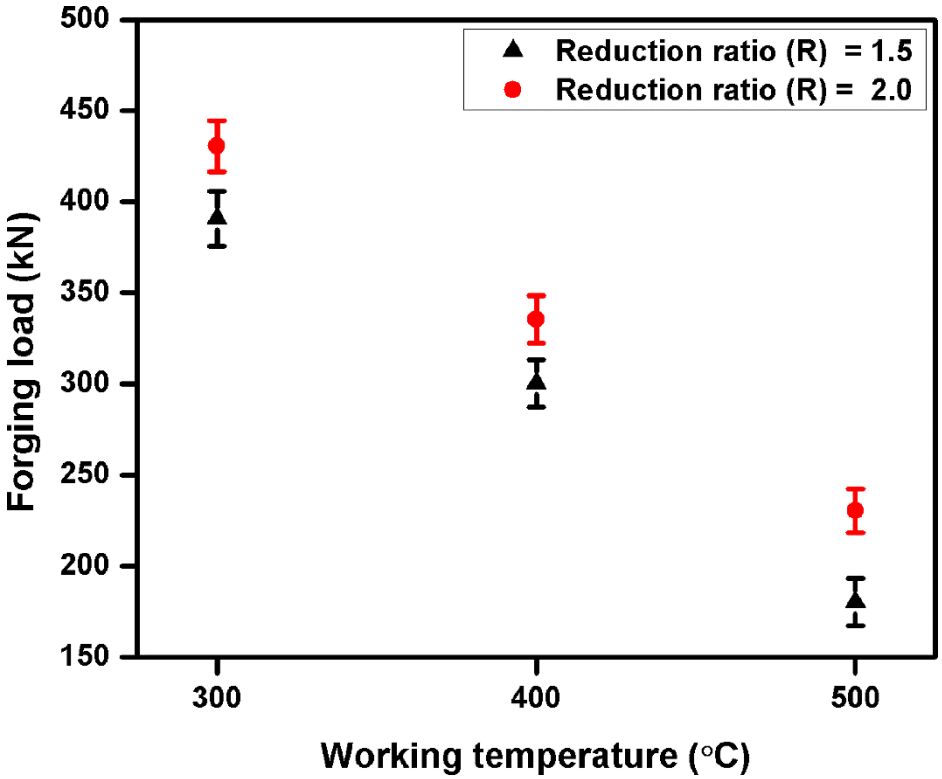

Figure 5.13 Forging load plotted against working temperatures for different reduction ratios

5.2.3 Microstructural features of forged complex hypoeutectic Al-7.4Si-2.5Cu-0.6Fe alloy

The effect of bulk processing on microstructural features of the forged alloy was investigated as per the discussion presented in the section 2.6. Figures 5.14-5.16 and Table 5.1 show the optical micrograph and average grain size of the forged samples at 1.20, 1.00, and 0.80 aspect ratios (h/d) and 300, 400, and 500°C working temperatures under lubricated and unlubricated conditions, respectively. The Figures 5.17(a-f) and Table 5.2 depict the optical micrographs and average Si grain size of the forged billet at reduction ratios (R) of 1.5 and 2.0 and 300, 400 and 500°C working temperatures.

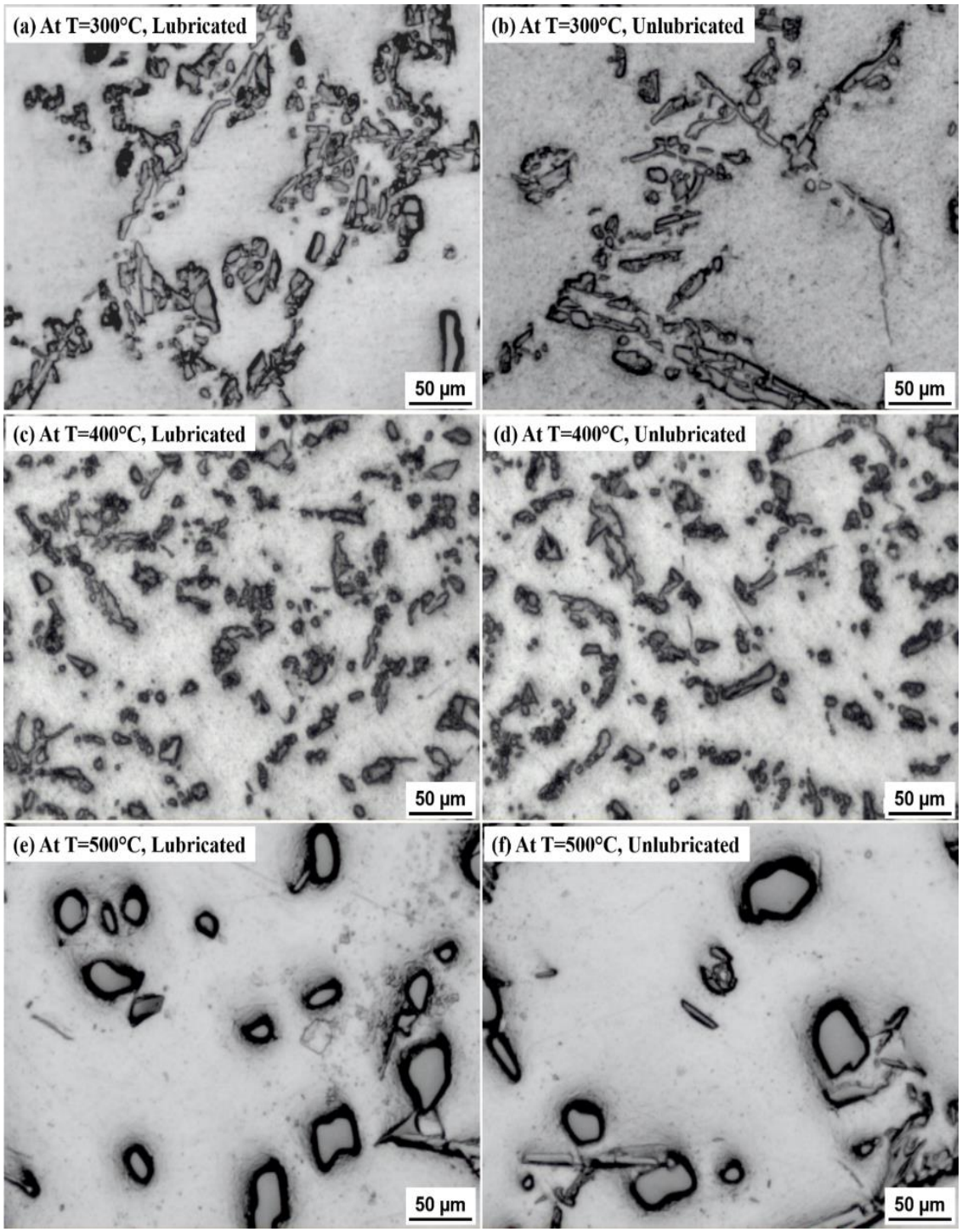

Figure 5.14 Optical microstructure of the forged samples at aspect ratio 1.20 under lubricated and unlubricated conditions

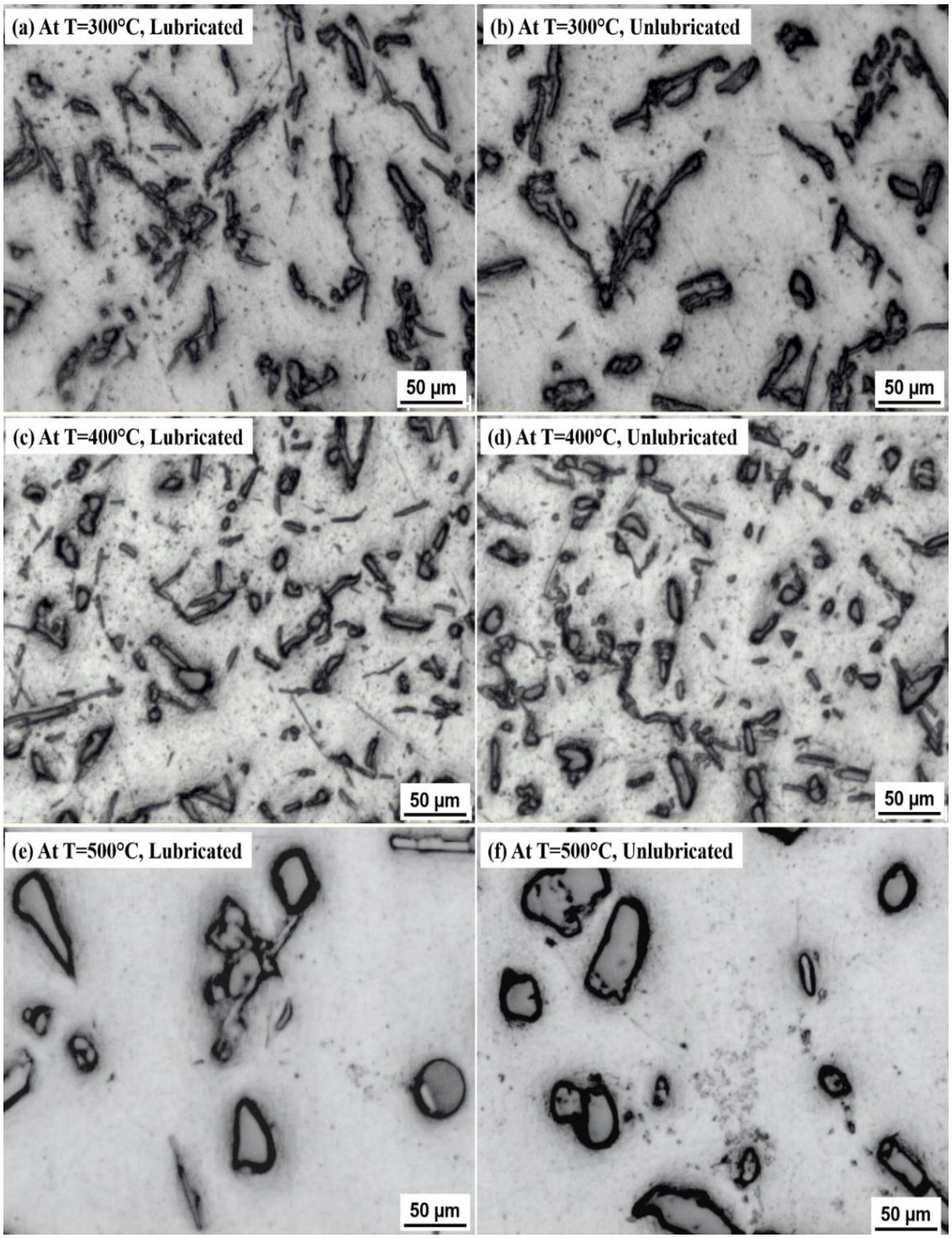

Figure 5.15 Optical microstructure of the forged samples at aspect ratio 1.0 under lubricated and unlubricated conditions

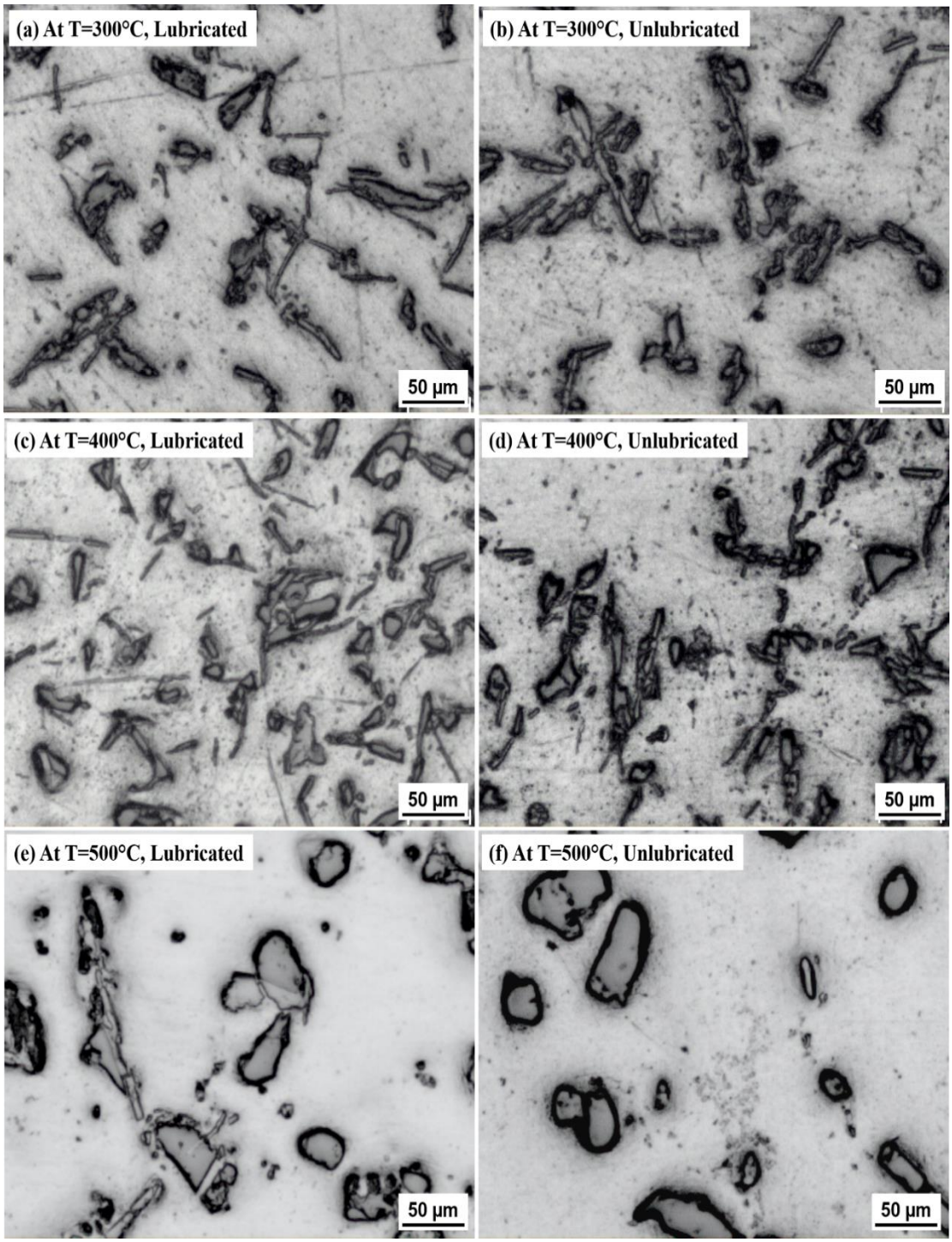

Figure 5.16 Optical microstructure of the forged samples at aspect ratio 0.80 under lubricated and unlubricated conditions

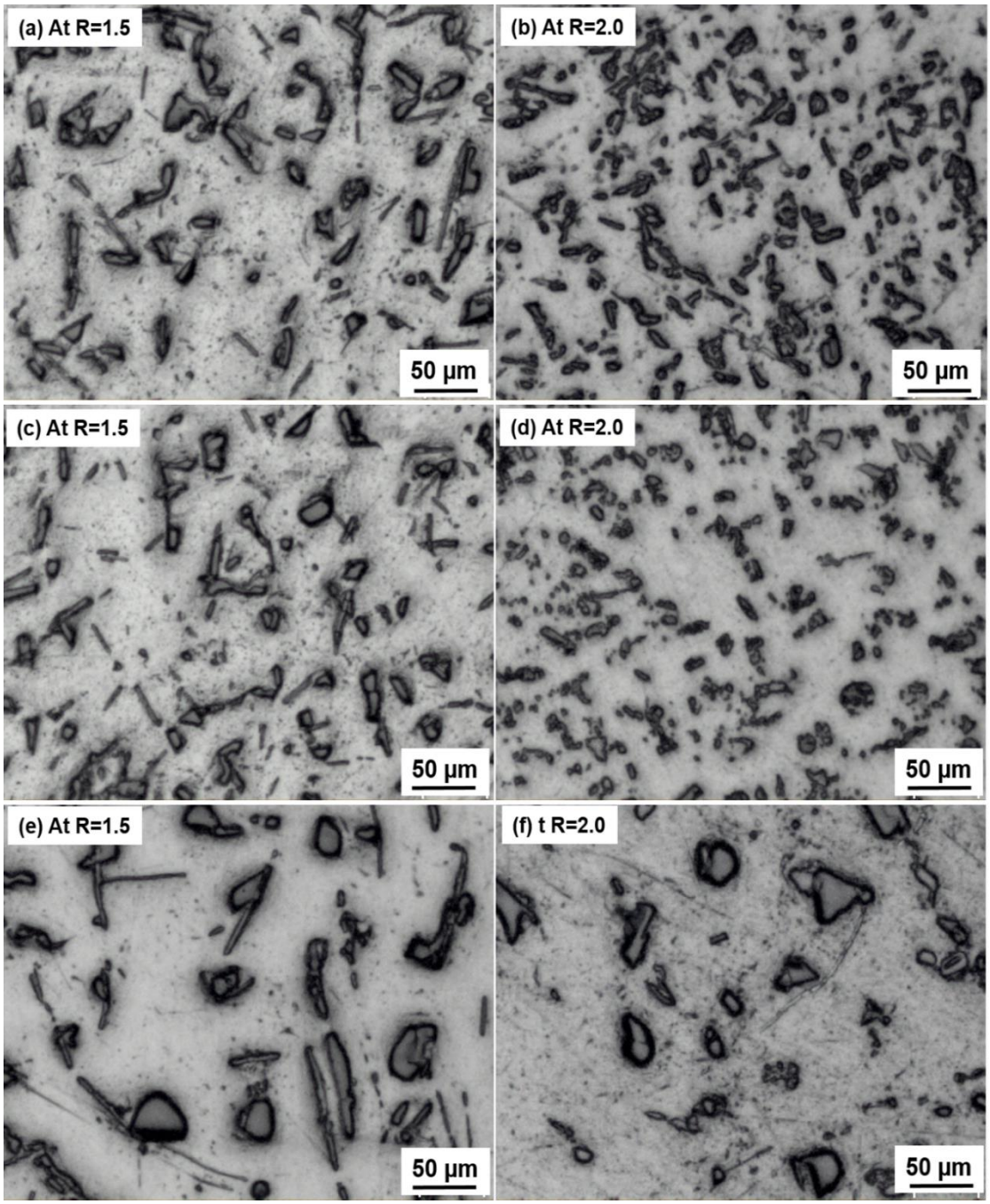

Figure 5.17 Optical micrographs of the forged billets (a) R=1.5, T=300°C, (b) R=2.0, T=300°C, (c) R=1.5, T=400°C, (d) R=2.0, T=400°C, (e) R=1.5, T=500°C, and (f) R=2.0, T=500°C

Table 5.1 Variation of average grain size of the eutectic silicon particle in forged samples under different processing conditions

Aspect Ratio (h/d)	Mean diameter/Standard deviation of the eutectic Si particles under different processing temperatures (μm)					
	300°C		400°C		500°C	
	Lub. cond.	Unlub. cond.	Lub. cond.	Unlub. cond.	Lub. cond.	Unlub. cond.
1.20	8.58/3.85	8.06/3.49	6.53/2.85	7.62/3.01	17.72/8.71	18.01/10.54
1.00	9.11/3.75	10.45/4.05	8.65/3.30	9.19/3.42	18.93/10.72	20.53/10.92
0.80	10.29/5.20	12.13/5.35	10.74/4.56	9.26/3.59	20.33/11.21	23.83/11.99

Table 5.2 Average grain size Si particles in forged samples at different processing temperatures

Forging temperature (°C)	Eutectic Si particles size at different reduction ratio (R)			
	R=1.5		R=2.0	
	Mean dia. (μm)	Stand. dev. (μm)	Mean dia. (μm)	Stand. dev. (μm)
300	8.42	2.38	6.45	1.97
400	7.17	2.15	6.35	1.83
500	9.30	2.85	8.08	2.38

Figures 5.14-5.17 reveal the microstructural refinement in forged samples during bulk processing of the alloy under various processing conditions. Tables 5.1 and 5.2 confirmed the reduction in eutectic Si grain size and it was higher at greater aspect and reduction ratios in impression and converging die forging, respectively. It may be attributed to greater degree of deformation at higher aspect or reduction ratios during forging. The results also show that refinement in Si grain was almost same in both lubricated conditions, and very slight variation in their size.

The microstructural refinement mechanism in the forged Al-7.4Si-2.5Cu-0.6Fe alloy was quite similar as discussed in previous sections 3.2.4 and 4.2.4. Prior to forging the homogenization of the test samples at pre-set processing temperatures rise the finer precipitate of the elemental alloying Si, Cu and Fe elements in α-Al matrix. While coarse

eutectic Si and hard intermetallic compounds failed to sustain higher applied deformation load during forging. Due to this, such second phase particles fractured in fragmented and uniformly dispersed in the α-Al matrix during bulk processing at elevated working temperatures. Therefore, bulk processing is a convenient way to alter the coarse cast microstructural features into the refined structures which subsequently enhances the tribo-mechanical properties of the processed material. The results show that microstructural refinement depend on the processing temperatures and it was increased as increase in the working temperature from 300 to 400°C as shown in Figures 5.14-5.17(a-d). As discussed in the previous sections 3.2.3 and 4.2.3 that more ductility gets induced in the alloy at high working temperatures which result severe deformation of the alloy during bulk processing. Due to this, more fragmentation and dispersion of the second phase particles take place. However, further increase in the working temperature from 400 to 500°C causes faster rate of diffusion of the Si atom which results in a coarsening of the Si particles during forging as shown in Figures 5.14-5.17(e-f).

Therefore, the bulk processing of the complex Al-7.4Si-2.5Cu-0.6 alloy at 300°C was found to be relatively low, while 500°C was relatively high working temperature during forging. Previously, various authors reported the similar microstructural refinement trends in the Al-Si alloys having different chemical compositions. They found that cast structure having coarse second phase particles destroyed with the application of the deformation load. Due to the applied load such brittle second phase fragmented into fine grains and uniformly distributed in the matrix. Thus, the alloy with equiaxed fine grain was produced through bulk processing by various investigators (Jamaati et al., 2011; and Mallpur et al., 2011).

5.2.4 Mechanical properties of the forged complex hypoeutectic Al-7.4Si-2.5Cu-0.6Fe alloy

5.2.4.1 Tensile strength of the forged alloy

Tensile tests of the as-cast and forged alloy were conducted according to experimental procedures as discussed earlier. The ultimate tensile strength (UTS) of the as-cast alloy was found to be 110±5 MPa. Figure 5.18 shows the engineering stress-strain profile of the as-cast and forged samples (lubricated conditions) with aspect ratio (h/d) 1.20 at 300, 400 and 500°C working temperatures. While Figure 5.19 shows the UTS of the forged alloy at different processing conditions. Figures 5.20, and 5.21 show the engineering stress-strain profiles of the as-cast and forged samples with reduction ratios (R) 1.5 and 2.0 at 300, 400 and 500°C working temperatures.

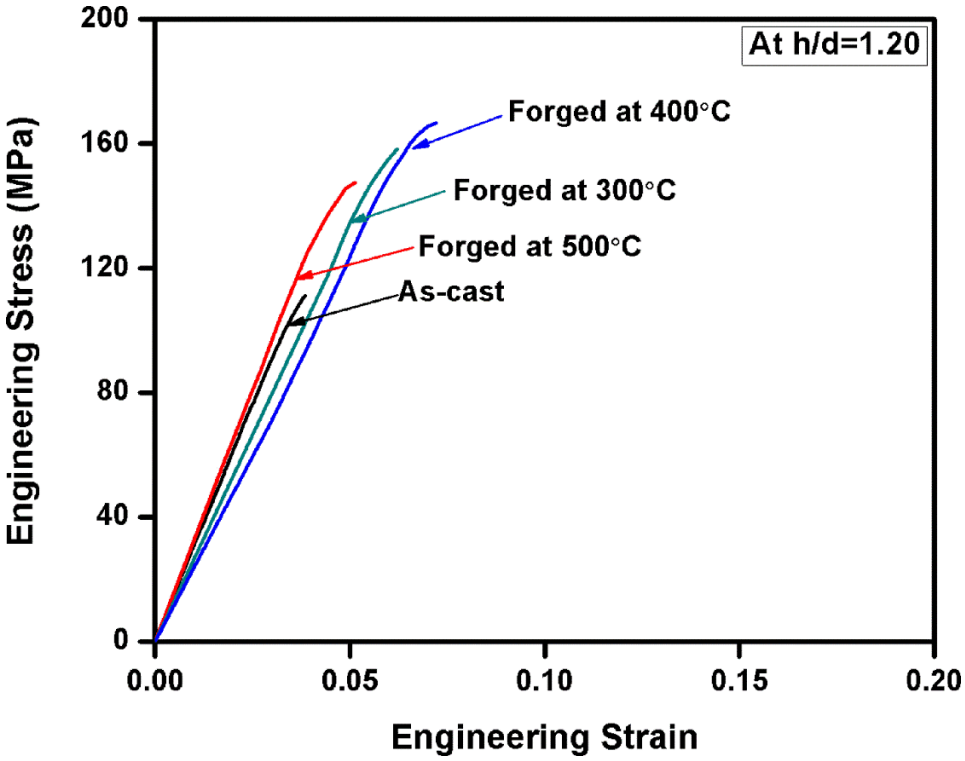

Figure 5.18 Stress-strain diagrams of the as-cast and forged samples (h/d=1.20)

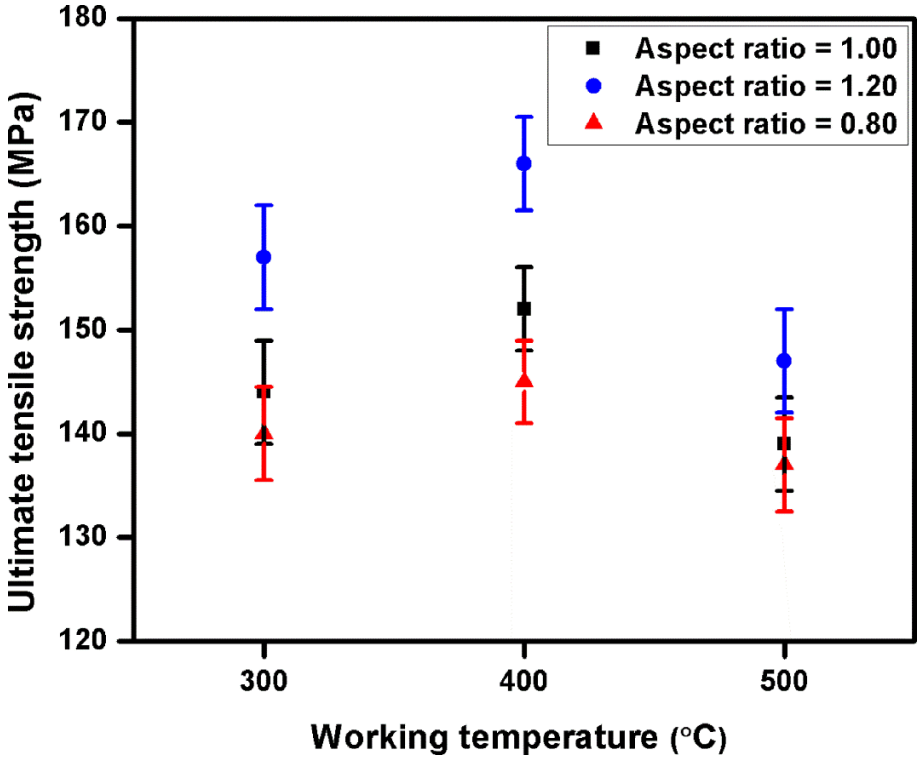

Figure 5.19 Ultimate tensile strength (UTS) of the forged samples shown against different h/d ratios and working temperatures (°C) under lubricated condition

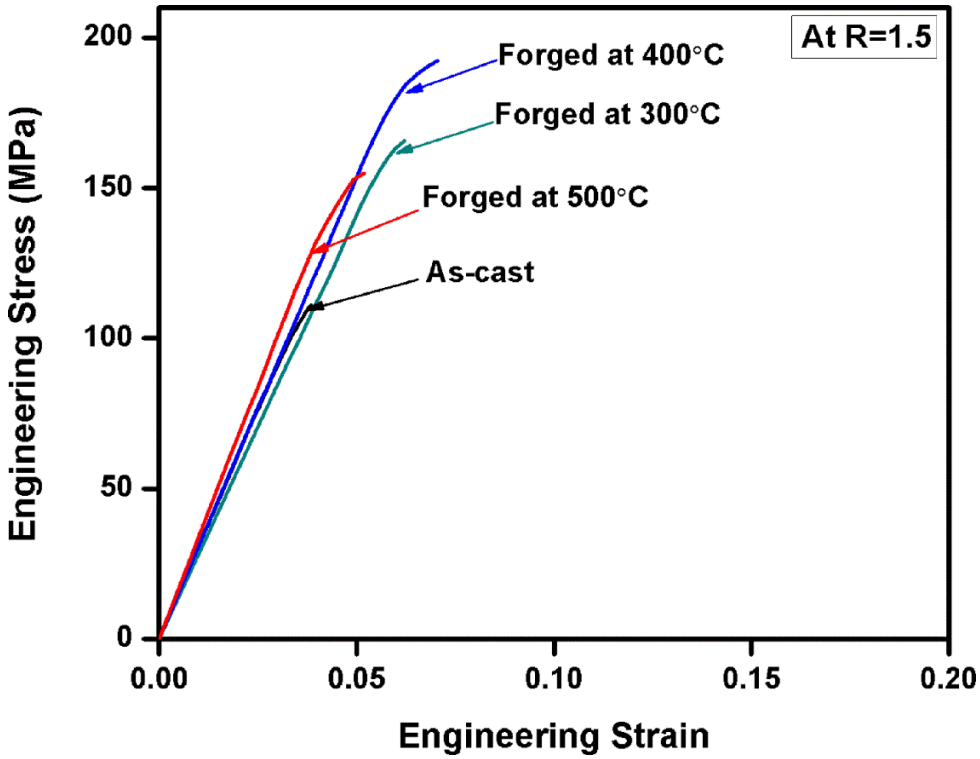

Figure 5.20 Stress-strain diagrams of the as-cast and forged samples (R=1.5)

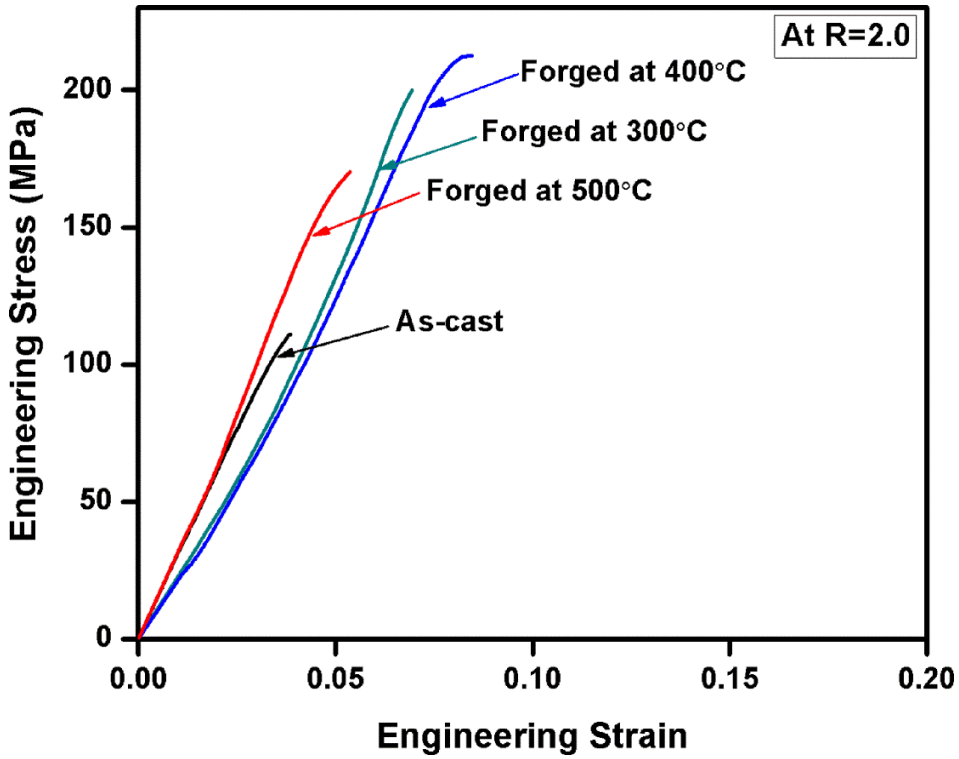

Figure 5.21 Stress-strain diagrams of the as-cast and forged samples (R=2.0)

The results reveal noticeable enhancement in tensile properties of the forged alloy in all test conditions as compared with as-cast alloy as shown in Figures 5.18-5.21. The as-cast alloy contains coarse needle shaped eutectic Si particles and hard intermetallic compounds as shown in Figure 5.3. Such coarse and brittle second phase particles lower mechanical properties of the alloy, and the material fails during initial loading conditions (Samuel et al., 2014). Therefore, such microstructural features should be modified to obtain the desired mechanical propitiates.

The results indicate the brittle failure of the tensile test samples in all processing conditions as shown in Figures 4.16, 4.18, and 4.19. It may be due to alloy having hard intermetallic compound of iron (β-$Al_{4.5}FeSi$) which deteriorates the mechanical properties of the alloy as reported in the previous sections. The XRD results also confirmed formation of complex β-

$Al_{4.5}FeSi$ compound in the alloy during solidification. Due to the presence of such hard intermetallic phases in the matrix, the material fails during straining without necking.

When the material was forged through different die conditions the high axial compressive load acted on the material during processing and thus the mechanical properties of the alloy enhanced. Due to this, the plastic incompatible second phase particles could not sustain such load and fragmented into fine grains and in turn developed strong bonding with Al matrix. Therefore, the material strengthens during bulk processing and shows considerable improvement in the tensile strength as shown in Figures 5.18-5.21.

Figures 5.18-5.21 also reveal that tensile strength of the forged alloy increased with increase in aspect or reduction ratio, and working temperature from 300 to 500°C. It is evident from previous section 5.2.3 that finer grains achieved at higher aspect ratio or reduction ratio which in turn significantly enhances the tensile strength of the forged alloy. However, due to the faster rate of diffusion and also grain growth of the matrix the increase in working temperature reduces the strength of the alloy due to coarsening of Si atoms The existing studies by various authors also confirmed the improvement in mechanical properties of the alloy processed through different other techniques. It may be reported that refinement in microstructural features noticeably improved the tensile strength of the processed alloy (Jamaati et al., 2011; and Mallpur et al., 2011).The decrement in tensile strength of the alloy was also confirmed due coarsening of the microstructural features at higher processing temperatures (Hagdadi et al., 2016).

5.2.4.2 Hardness

Hardness of the as-cast and forged alloy was measured through Vicker's microhardness tester at 100 g indentation load and 10 sec dwell time. The hardness of the as-cast was found to be 44±4 HV. Figures 3.27 and 3.28 show the hardness value of the forged alloy through

impression die and converging die, respectively. The results indicate significant improvement hardness of the forged alloy as compared with as-cast alloy in both the forging conditions. The strengthening mechanisms were discussed in section 5.2.4.1 also explain the improvement in hardness of the forged alloy at different processing conditions. Increase in the dislocation density and more uniform dispersion of the second phase particles in Al matrix during forging enhances the hardness of the alloy. Figures 5.22 and 5.23 reveal that hardness of the forged alloy increased with increase in the aspect ratio or reduction ratio and working temperatures form 300 to 400°C. While the decrement in hardness of the alloy due to coarsening of the microstructural features the alloy forged at 500°C. Therefore, 300°C found to be relatively lower and 500°C was relatively higher bulk processing temperature to get desired results.

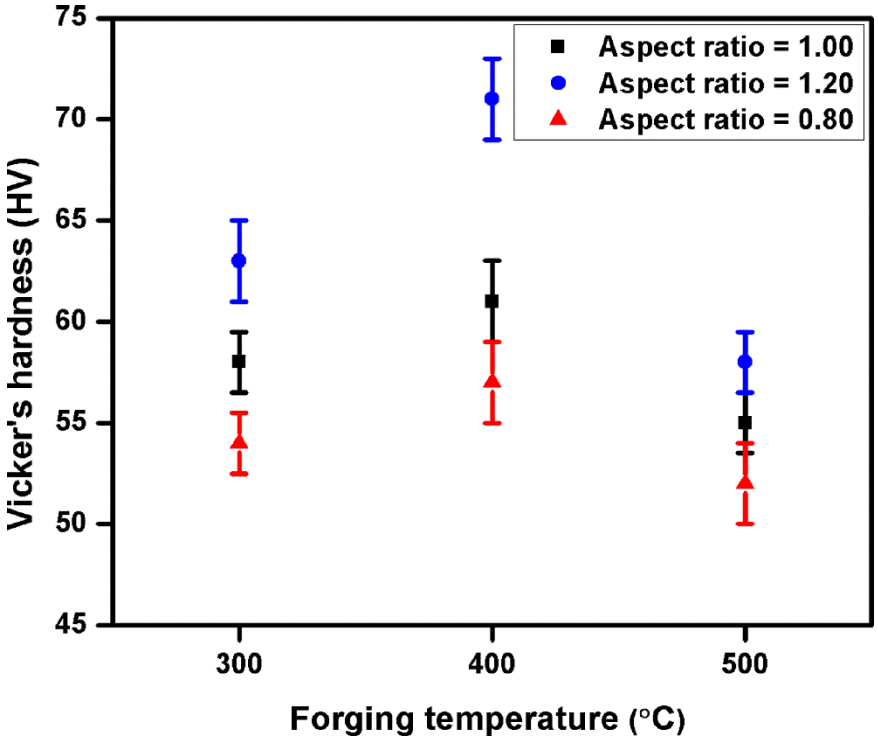

Figure 5.22 Vicker's microhardness of the forged samples shown against different h/d ratios and working temperatures (°C)

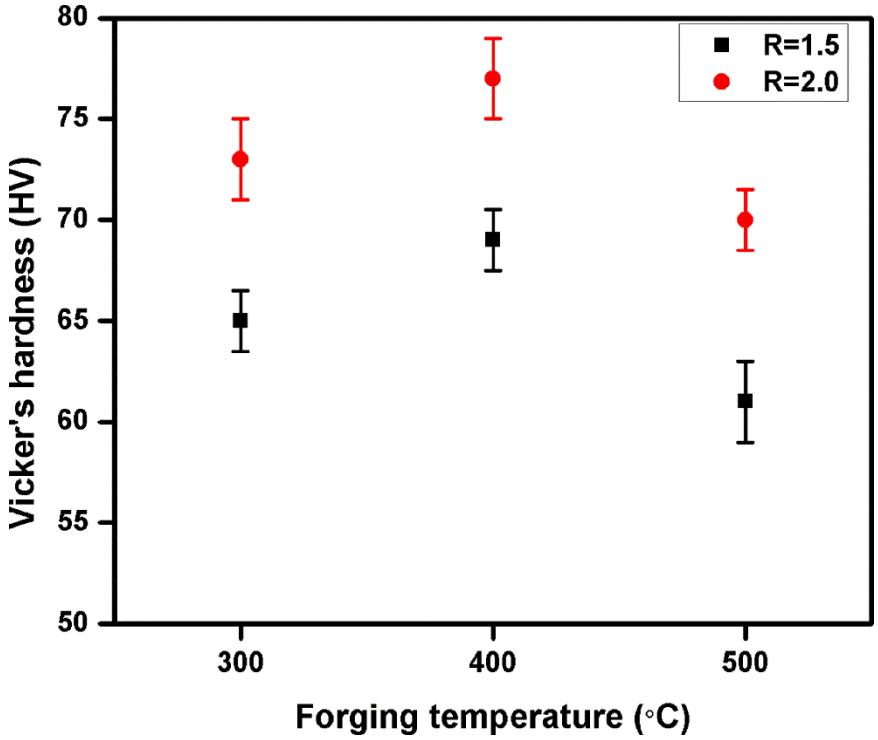

Figure 5.23 Vicker's microhardness of the samples forged to different reduction ratios (R) of 1.5 and 2.0 at different working temperatures

The existing investigations by various authors have also confirmed the improvement in hardness of the processed alloy. It may be reported that uniform dispersion of the second phase particles in the matrix and higher dislocation density generates during high strain rate deformation significantly improved the hardness of the alloy (Jamaati et al., 2011; and Mallpur et al., 2011).

5.2.4.3 Fractography

Figure 5.24 shows the SEM images of the fracture surface of the failed tensile samples at room temperature. The fracture morphology of the as-cast alloy confirmed the brittle mode failure, and the sample failed with almost negligible plastic deformation due to presence of hard silicon particles. During straining, the stress concentration generated between α-Al matrix and needle shaped eutectic Si particles which results initiation and propagation of

cracking along the grain boundary. Due to this premature failure of the samples without attained the intrinsic strength.

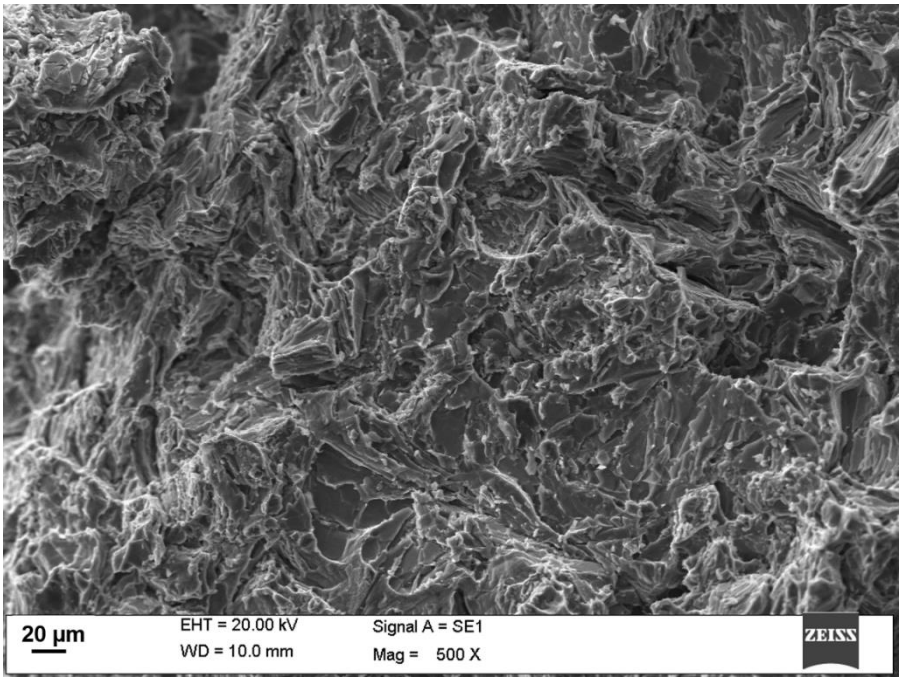

Figure 5.24 SEM image of the as-cast tensile fractured surface

The fracture morphology of the forged samples with aspect ratio (h/d) of 1.20 and reduction ratio (R) of 2.0 at 400°C forging temperature is as shown in Figures 5.25(a) and (b). The fractured surface of the forged samples also show the brittle mode failure with very minute plastic deformation. It may be due to needle shaped second phase compounds got modified into fine particles which in turn minimize the stress concentration between α-Al matrix and second phase particles. However, it was not sufficient to obtain the desired strength of the material, and the test sample failed before reaching the intrinsic point. Therefore, the fracture surface also shows the presence of very few shallow dimples. In earlier investigation by various authors show that Al-Si alloy with low Si wt.% failed due to ductile fracture during straining. It may also be reported that presence of needle shaped Si particles and intermetallic phases in the soft Al matrix reduces the tensile properties of the alloy. Such second phase

particles developed high stress concentration with Al matrix during straining, and creates micro-cracks with further propagate and grow until the failure during straining (Moffat et al., 2005).

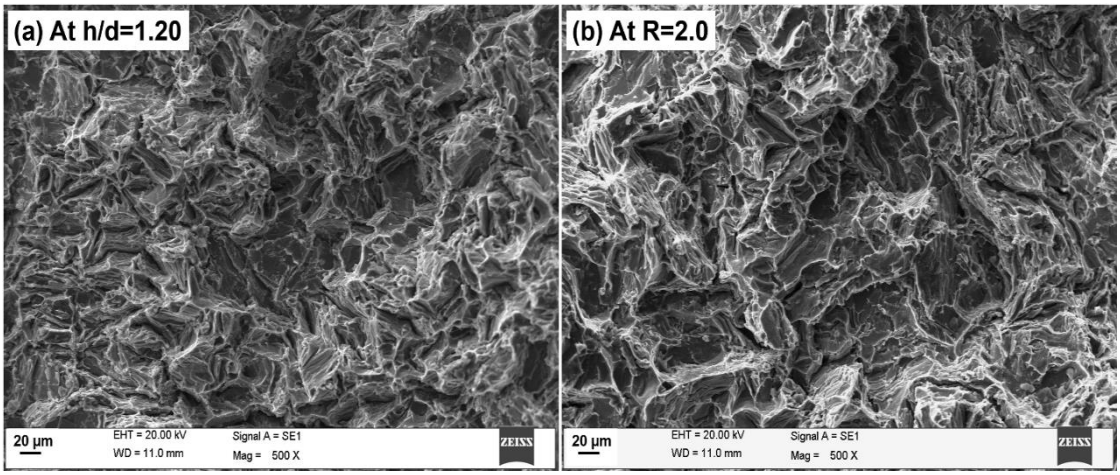

Figure 5.25 SEM images of the fractured surface of the samples forged at 400°C under (a) aspect ratio h/d=1.20, and (b) reduction ratio R=2.0

5.2.5 Wear behavior of the as-cast and forged complex hypoeutectic Al-7.4Si-2.5Cu-0.6Fe alloy

To investigate the effect of the processing parameters on wear characteristics of the bulk processed alloy under dry sliding conditions, a pin on disc tribometer was used. The results reveal that microstructural features and mechanical properties of the forged alloy considerably improved as compared to as-cast alloy during bulk processing in both the die setups. The forged alloy shows almost similar mechanical properties, while the sample forged through converging die shows more refined microstructure as compared to impression die. Therefore, sample processed from converging die forging were prepared for wear test. The existing studies by various investigators reveal that wear resistance of material depends on its microstructural features and hardness value (Alidokht et al., 2012; and Lee et al., 2012).

5.2.5.1 Wear behavior of the as-cast and forged complex hypoeutectic Al-Si alloy through converging die

Figures 5.26 and 5.27.show the variation in cumulative weight loss against sliding distance of the as-cast and forged samples with reduction ratios (R) of 1.5 and 2.0 under applied normal load of 20 N. The results reveal that cumulative weight loss increases with increase in sliding distance for all the test samples. Initially the weight loss was low but it was increased abruptly with further increase in the sliding distances. The results indicate weight loss was minimum for forged samples specifically for 400°C as compared to as-cast alloy. It may due to higher hardness value of the forged alloy which reduces the mass loss during sliding.

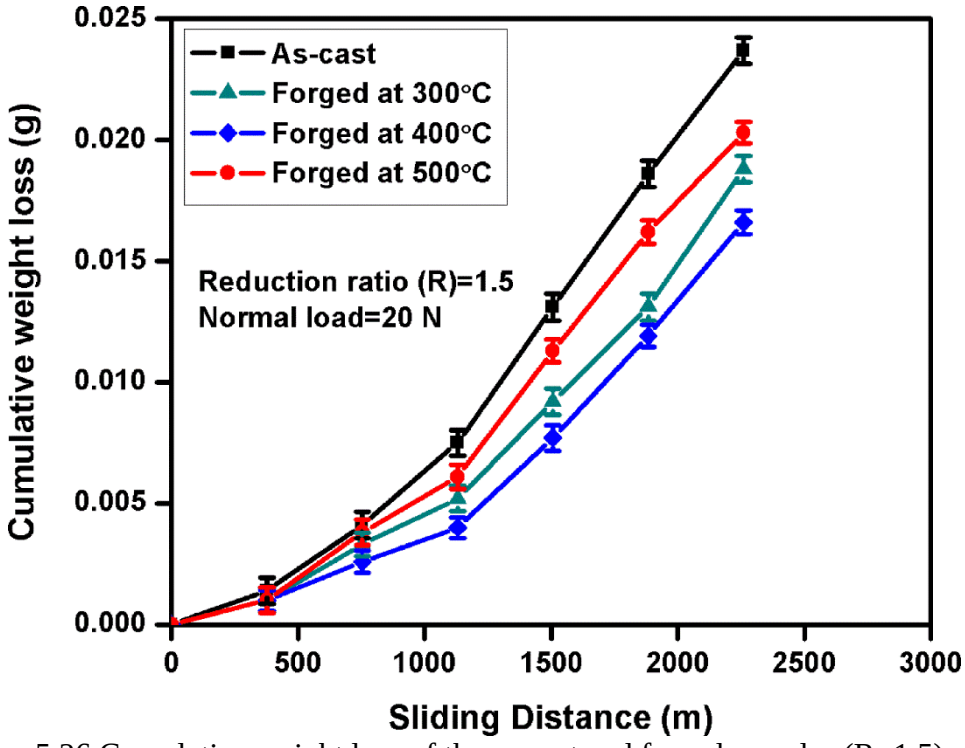

Figure 5.26 Cumulative weight loss of the as-cast and forged samples (R=1.5) under different conditions

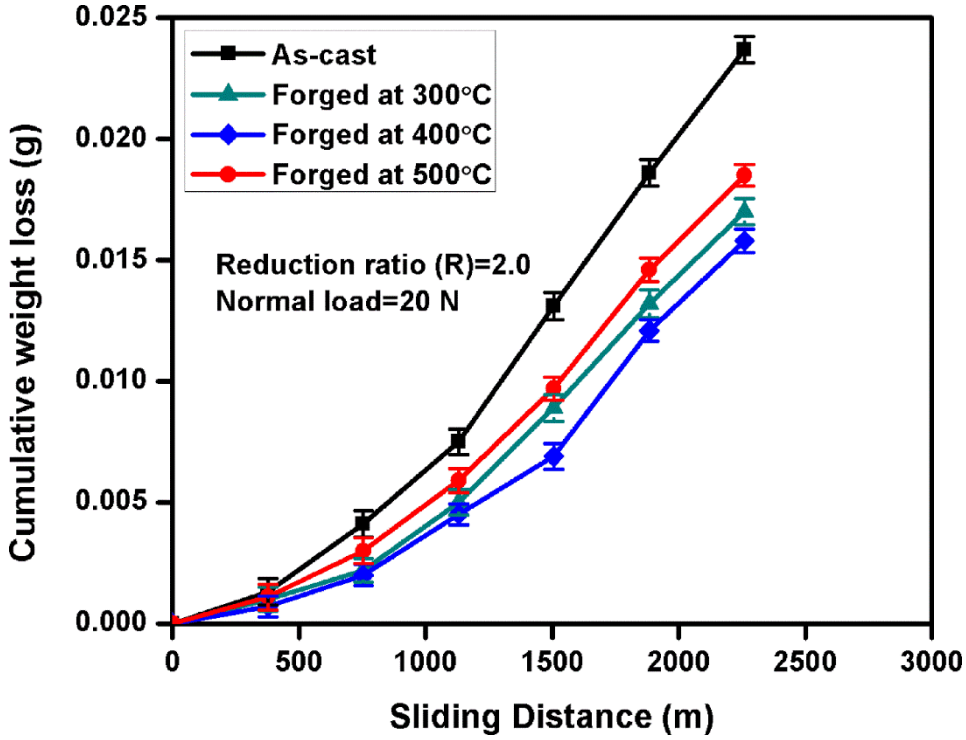

Figure 5.27 Cumulative weight loss of the as-cast and forged samples (R=2.0) under different conditions

Figures 5.28 and 5.29 show the variation of wear rate with the applied normal load for the as-cast and forged samples with a reduction ratio of R=1.5 and 2.0 at 300, 400 and 500°C working temperatures. The wear test of all samples was performed for constant sliding velocity and distance of 1.3 m/s and 2260 m respectively, under the dry sliding condition at room temperature. The results indicate that wear resistance of the material considerably increased during bulk processing in all conditions. The as-cast alloy shows severe weight loss during dry sliding against the counter disc, and it was greater for higher applied normal load of 30 N. It may be due to low hardness value and coarse microstructural features of the as-cast alloy which in turn lead to severe plastic deformation and detachment of the pin material as wear debris. As discussed in the earlier section that the hardness of the alloy enhanced during bulk processing which reduces the material loss of the pin. Therefore the forged samples of Al-7.4Si-2.5Cu-0.6Fe shows improved wear resistance during dry sliding.

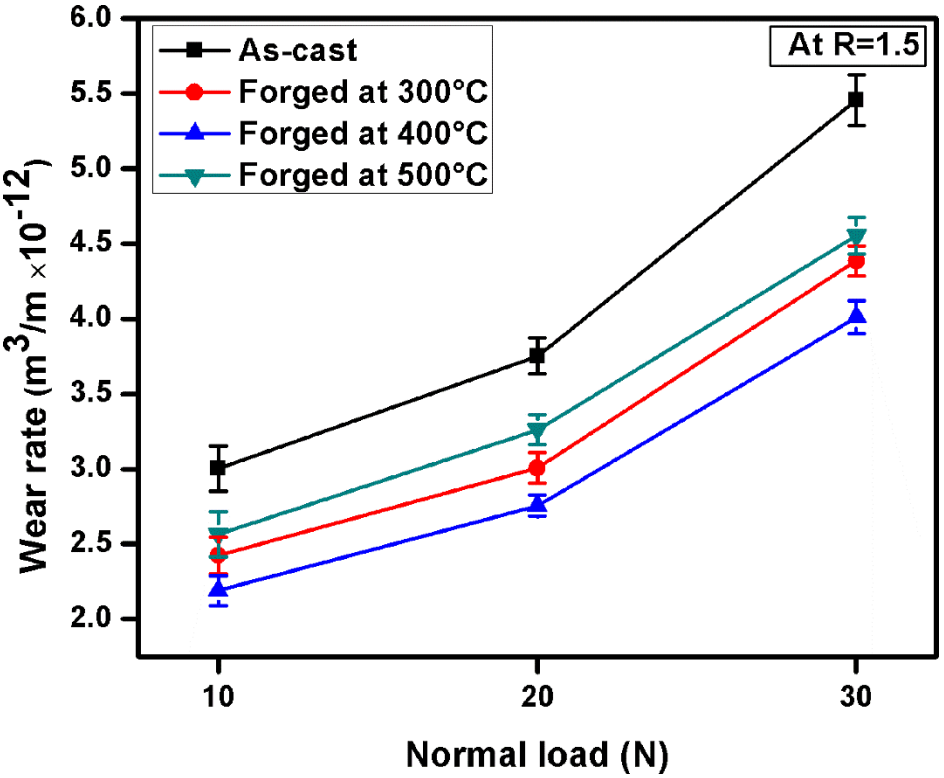

Figure 5.28 Wear rate of the as-cast and forged samples at R=1.5 and 10, 20, 30 N normal loads

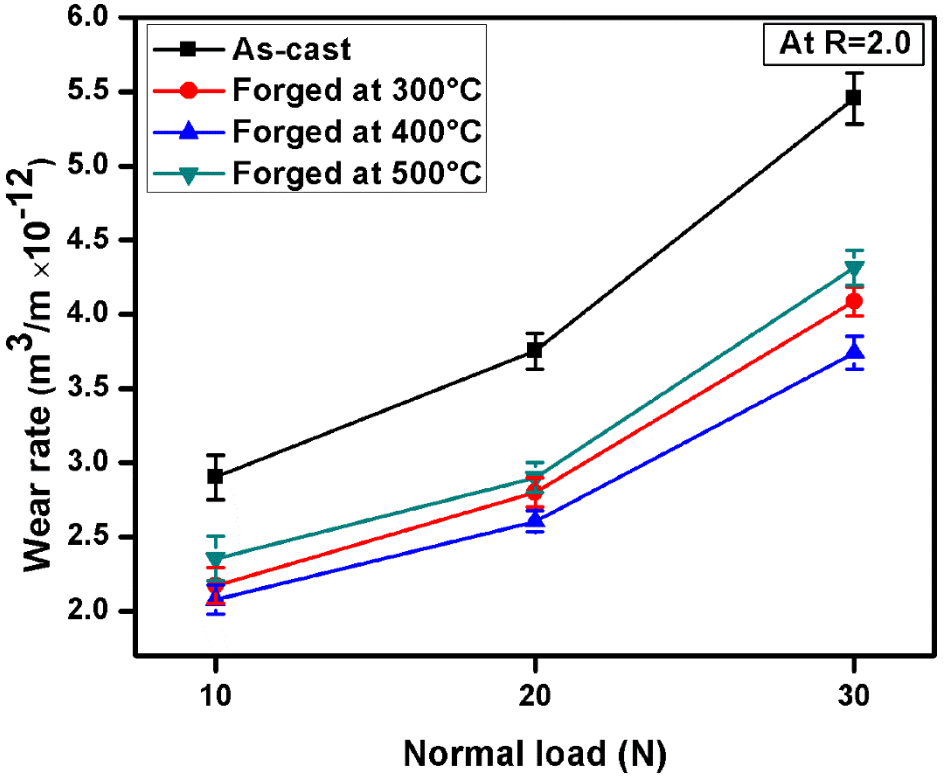

Figure 5.29 Wear rate of the as-cast and forged samples at R=2.0 and 10, 20, 30 N normal loads

Figures 5.28 and 5.29 also indicate that wear rate of the forged samples decreased with increase in the reduction ratios and processing temperature from 300 to 400°C while it decreased when processing temperatures increase from 400 to 500°C. It may be due to improvement in microstructural features and mechanical properties of the material due to increase in the processing temperatures. However, coarsening in microstructure occurred at higher processing temperature (500°C) during forging which in turn reduces the tribo-mechanical properties of the forged alloy. The existing study also confirms the similar wear trend in other hypoeutectic Al-Si alloys (El Aal and Kim, 2014).

5.2.5.2 Wear Mechanism

Figures 5.30 and 5.31 depict the worn surface morphology of the as-cast and forged samples. Figures 5.30(a-f) show the worn surface morphology of the as-cast and forged samples (R=1.5 and 2.0 at 400°C) at constant normal load and sliding speed of 20 N and of 1.3 m/s, respectively for different sliding distances of 755 and 2260 m. Figures 5.30(a-f) indicate that the volume mass loss increases with increase in the sliding distance and the worn surface morphology changes from mild to severe wear. The worn surfaces show the narrow grooves and scratches at small sliding distance, while wider and deeper grooves were formed on the pin surfaces at higher sliding distance as shown in Figures 5.30 (a-f). The above worn morphology trend show that abrasion and adhesion was the primary wear mechanism responsible for the material loss in the test alloy.

As discussed earlier, due to localized friction heat generated during sliding increases with increase in the sliding distance. Due to this, a substantial heat generation between the rubbings surfaces occurred which led to the softening of the alloy occurs and reduces the yield strength of the material. Thus, the soft material gets deformed plastically during sliding, which increases the adhesive wear of the pin, and transfer the material to the counter surface.

Wider grooves were observed at higher sliding distance as can be seen in Figures 5.30 (b, d and f). During this period, oxide layer was formed between the contacting surfaces which peeled out due to abrasion during sliding and expose the sub surface.

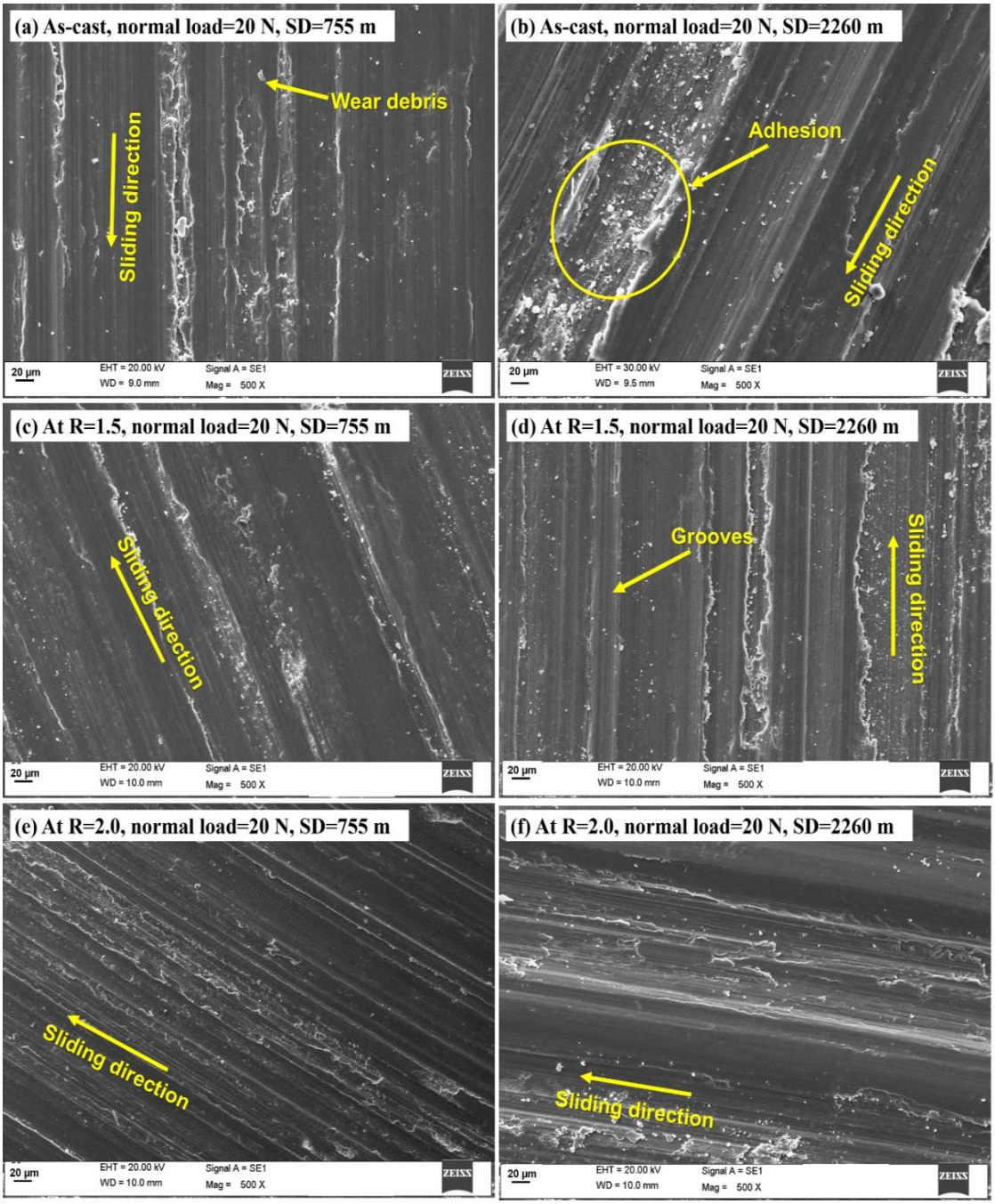

Figure 5.30 Worn surface morphology of the as-cast and sample forged at 400°C, at constant applied normal load of 20 N, sliding velocity of 1.3 m /s for different sliding distances

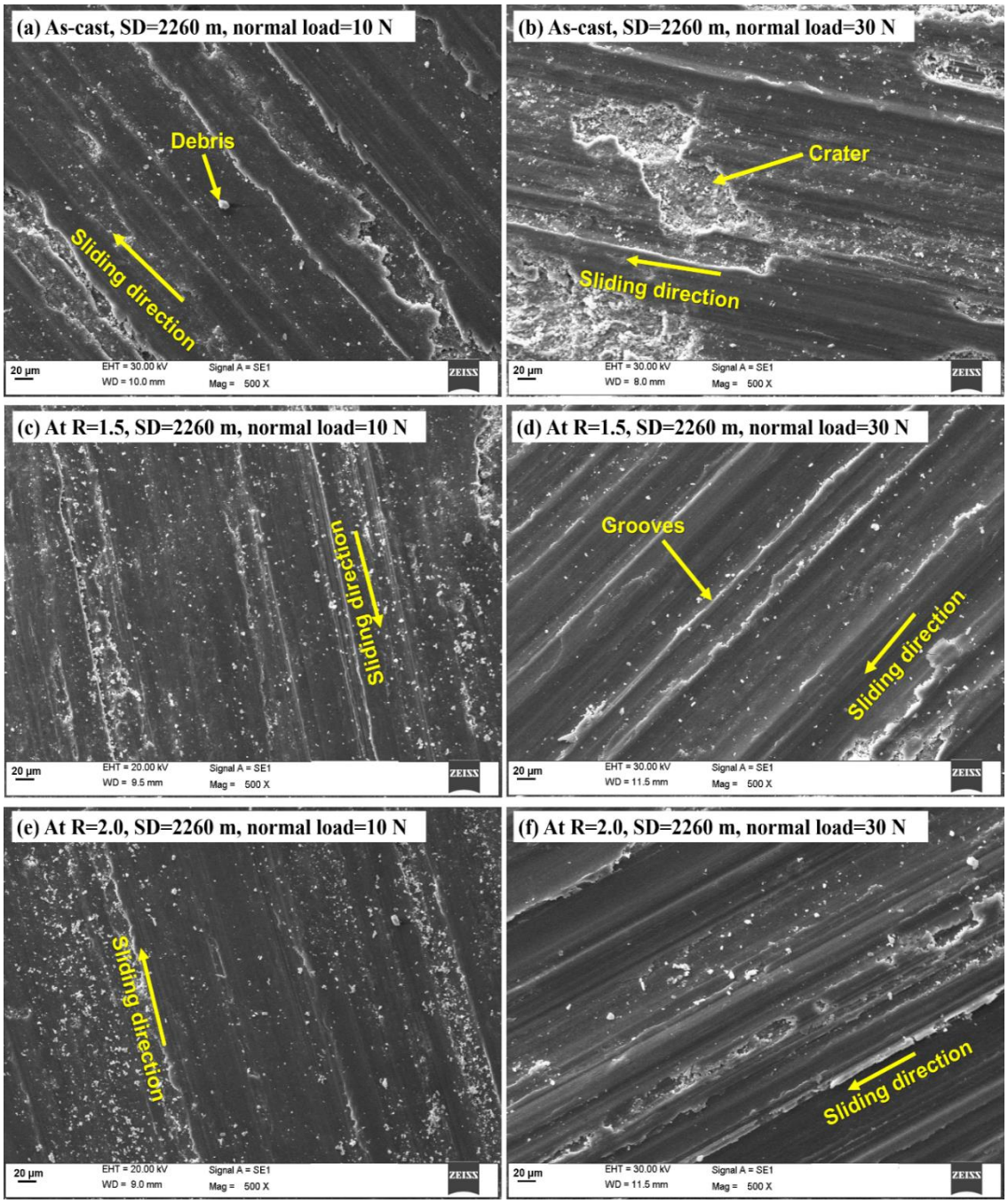

Figure 5.31 Worn surface morphology of the as-cast and samples forged at 400°C, at constant sliding distance of 2260 m, sliding velocity of 1.3 m /s for different applied normal loads

The results reveal that as-cast alloy shows poor worn surface morphology as compared to the forged alloy as seen in Figures 5.30 (a-f). It may be due to coarse microstructure and lower hardness of the as-cast alloy which lead to easily wear of the material, while the forged

alloy having a refined microstructure which enhances the hardness of the alloy, and in turns wear resistance of the alloy.

A similar trend was also reported earlier that increase in sliding distance generates severe friction between the contacting pin and the counter disc, which results in high wear of the alloy and consequently produces severely worn surface morphology (Alhawari et al., 2015; and Pramod et al., 2015). The previous studies also reveal that material with coarse microstructure and low hardness show poor wear resistance. The alloy having coarse needle shaped eutectic Si and intermetallic compounds generate stress concentration in the Al matrix and increase the internal stress in the pin material during sliding. Due to this, cracks and micro-cracks were developed on the pin surfaces and thus the interconnection of these cracks produce bulk amount of the mass loss as detachment of wear debris.

Figures 5.31(a-f) show the worn surface morphology of the as-cast alloy and the forged samples (R=1.5, 2.0 and 400°C) at a constant sliding distance of 2260 m and sliding speed of 1.3 m/s for different applied normal loads of 10 and 30 N.

The results reveal that the severity of the worn surfaces increases as the applied normal load was increased from 10 N to 30 N as shown in Figures 5.31 (a-f). Further, also the deep penetration of the hard asperities of the counter surface to the soft pin surfaces at higher load. It may be due to high localized frictional heat generation during sliding which softens the alloy and enhances the tendency to deform the material plastically, because at higher applied load, the pin exerts more pressure on the disc and tried to stop the sliding motion. Therefore due to severe friction, the heat gets generate between the contacting surfaces which deformed the soft material plastically and produces wider and deeper grooves as shown in Figures 5.31(a-f). This increases the adhesion between contacting surfaces.

In addition some micro-cracks and cracks were formed due to abrasion during sliding which interconnected with each other and produce crater on the surfaces. During sliding the oxide layer was formed between interacting surfaces which prevent the direct exposure of the pin material during sliding. While the protective oxide layer was broken down due to action of higher applied pressure, the pin surface again rubbed with hard counter surface and worn out during sliding. Therefore, pin material weld on the counter surfaces and detached in the form of wear debris and act as third body abrasives in contacting surfaces. The results reveal that severity of wear is decreased for the forged samples as compared to as-cast alloy as seen in Figures 5.31(a-f). It may be due to improved hardness and microstructural features in the forged alloys, and it was higher for the sample forged at higher reduction ratio (R=2.0). The above results reveal that the wear resistance of the material depends on the hardness and microstructural features of the alloy. The existing studies by various investigators have also shown similar wear trend in hypoeutectic Al-Si alloys having other chemical composition. It may be reported that wear rate was noticeably increased at higher applied pressures which in turns severity of the worn surfaces enhanced produces deeper grooves and craters (Kori and Prabhudev, 2011; and Van Thuong et al., 2015).

Figures 5.32 and 5.33 depict the EDS spectrum of the worn surface of the as-cast and forged alloy (R=2.0 at 400°C) at 30 N normal load and sliding distance of 2260 m. The EDS spectrum of both the worn surfaces of the test samples contains Al, Si, Cu, and Fe elements along with oxygen during dry sliding between interacting surfaces. The presence of the Fe in the worn surface confirmed the material transfer from counter surface, while oxygen indicates the oxidation of the surfaces during dry sliding.

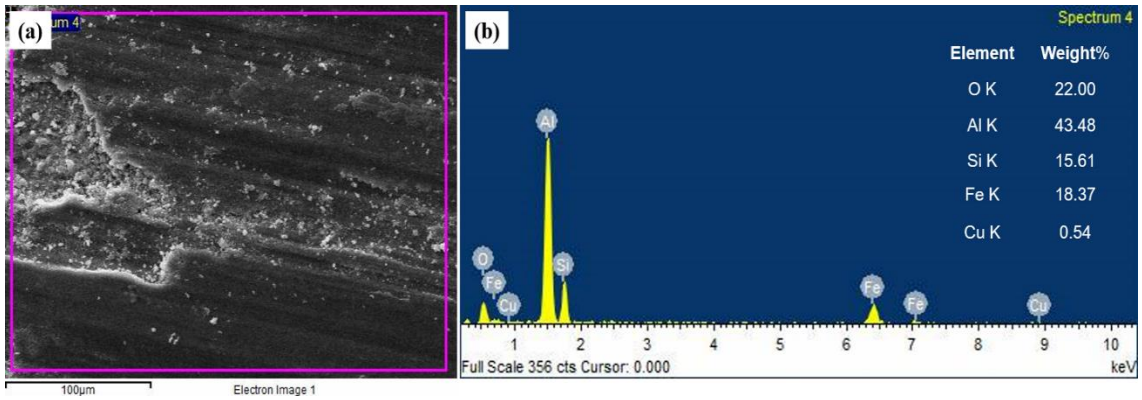

Figure 5.32 EDS analysis of the worn surface of the as-cast alloy at 30 N normal load and sliding distance 2260 m

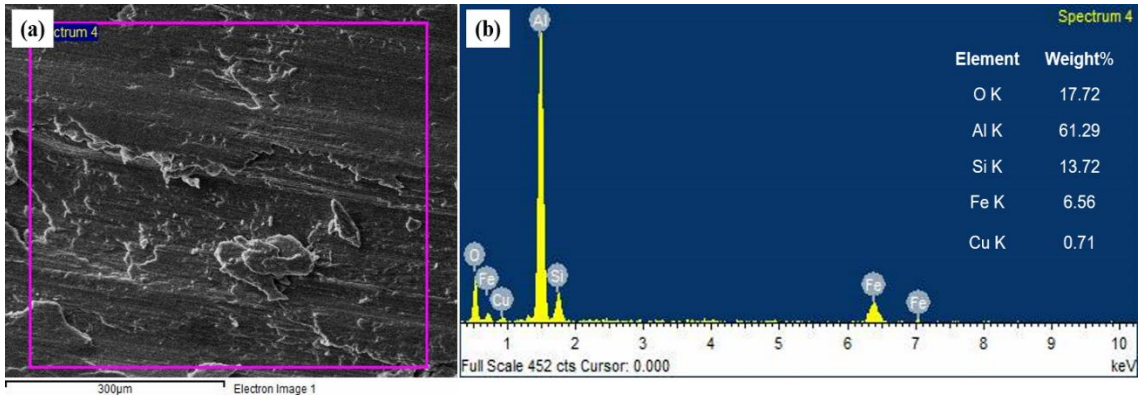

Figure 5.33 EDS analysis of the worn surface of the sample forged at R=2.0 and 400°C at 30 N normal load and sliding distance 2260 m

5.2.5.3 Roughness measurement

Figure 5.34 shows the three dimensional AFM images and their respective roughness profiles of the worn surfaces of the as-cast and forged alloy with reduction ratios (R) 1.5 and 2.0 for the scanning area of 50 µm × 50 µm for each sample.

The AFM analysis of worn surfaces was performed to evaluate the root mean square (rms) roughness (Rq) of the as-cast and forged samples. It was found to be 0.705 µm for the as-cast worn sample which indicates the poor surface roughness produced during dry sliding. The surface roughness (Rq) of the forged worn surfaces was found to be 0.503 and 0.421 µm

for samples with 1.5 and 2.0 reduction ratios, respectively as shown in Figures 5.34(b) and 5.34(c).

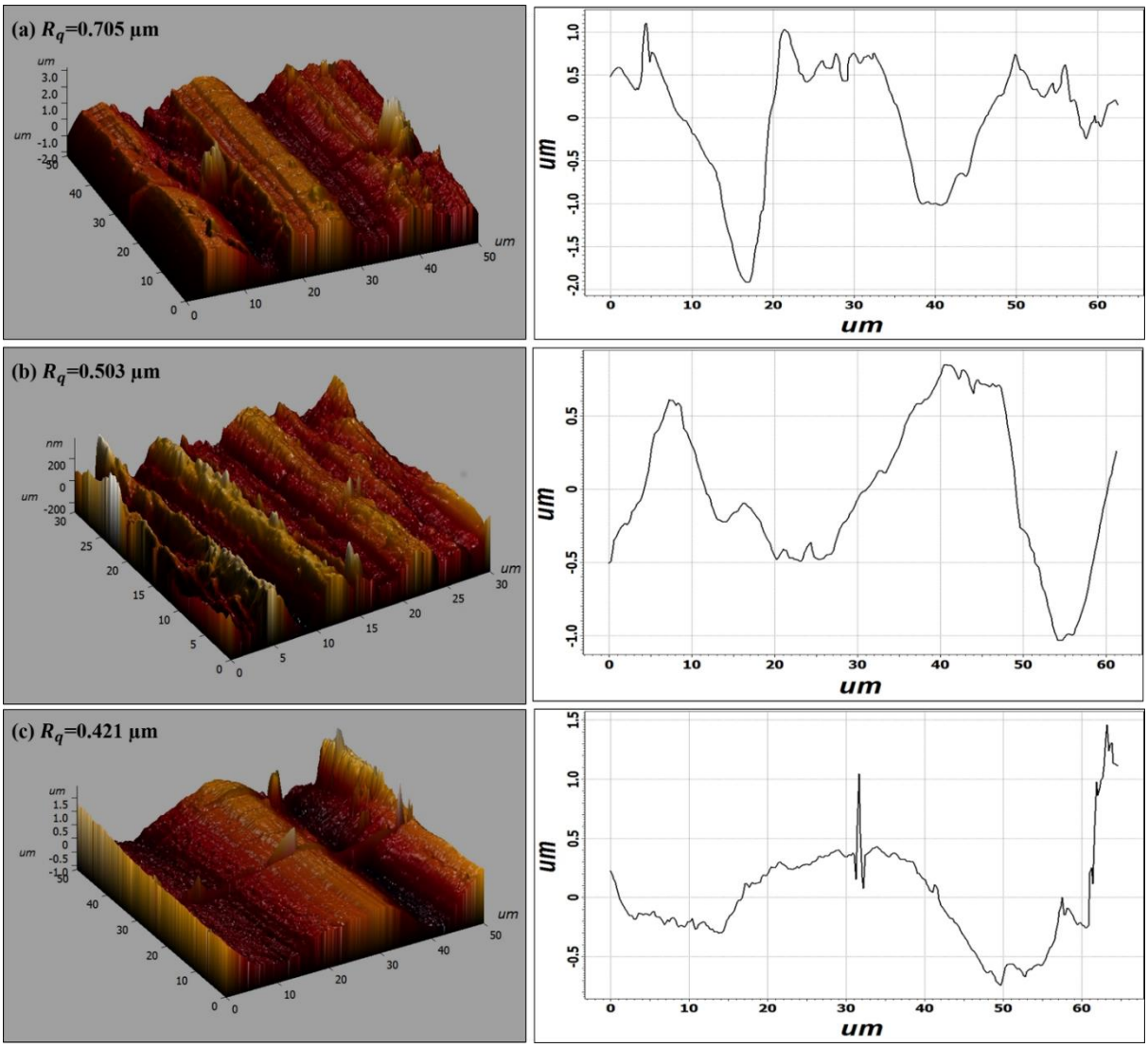

Figure 5.34 AFM morphology of worn surfaces at sliding distance of 2260 m, sliding velocity of 1.3, and applied normal load of 20 N for the different samples (a) as-cast, (b) forged R=1.5 at 400°C, and (c) forged R=2.0 at 400°C

The results reveal that as-cast sample shows poor worn surface roughness, while it was improved for forged samples. As reported in earlier section that material having higher hardness value possess resistance to plastic deformation, which reflect the less wear of the samples during dry sliding. Archard's law also confirms the less wear of the material having

higher hardness value, which in turn possess better surface morphology of the sliding metal surfaces (Alemdağ and Beder, 2014). The results also reveal that surface roughness of the material decreased when the reduction ratio is increased. The roughness profile shows that peak height and depth of penetration was very high for as-cast worn sample, and it was found to be ≈1915 and ≈1105 nm as shown in Figure 3.32(a). The forged sample indicates reduced peak height and depth of penetration, and found to be ≈743 & ≈1458 nm for sample with R=1.5 and ≈1033 & ≈849 nm for R=2.0 as shown in Figures 5.34(b) and 5.34(c), respectively. It may be attributed to the low surface roughness of the forged worn samples which reflect the low peak height and depth of the penetration.

5.3 Summary

In this studies different bulk processing techniques such as open die, impression die and converging die forging have been performed to investigate the deformation behavior of the complex Al-Si alloy (Al-7.4Si-2.5Cu-0.6Fe) and its effect on the microstructural features, mechanical properties and wear characteristics of the forged alloy. The important findings are summarized below:

1. Very few minute surface cracks were observed in the forged products during open die forging of the alloy at a room and elevated processing temperature.
2. The smooth and crack-free product obtained during impression die forging of the test samples having different aspect ratios (h/d=1.20, 1.00 and 0.80) at room temperature in the both lubricated and unlubricated interfacial friction conditions
3. The impression die forging of the test samples having different aspect ratios (h/d=1.20, 1.00 and 0.80) processed at elevated temperatures (300°C, 400°C and

500°C) also produces crack free sound forged products in the both lubricated conditions.

4. The converging die forging test samples through two different reduction ratios of 1.5 and 2.0 also produce defect free sound forged products under elevated processing temperatures (300°C, 400°C and 500°C).
5. Forging load increased with increase in aspect ratios in impression die and reduction ratio in converging die forging, while it reduces when increasing the processing temperatures.
6. The microstructural featured of the forged alloy refined significantly during bulk processing through impression die and converging die forging under various processing conditions.
7. Such improvement in microstructural features enhanced the tensile strength, hardness and wear resistance of the forged alloy and it was higher the samples with an aspect ratio of 1.20 in impression die, and 2.0 reduction ratio in converging die forging. Coarsening occurred in the microstructural features at 500°C processing temperature during forging.
8. SEM images of the worn surfaces reveal that adhesion, abrasion and oxidation were the dominant wear mechanism in the as-cast and forged samples. AFM analysis depicts that surface roughness was minimum for the forged samples.

The next chapter 6 present the comparative studies of the bulk processed complex Al-Si alloy.